Control strategies for atmospheric pressure plasma polymerization of fluorinated silane thin films with antiadhesive properties

Article type: Research article

Title: Control strategies for atmospheric pressure plasma polymerization of fluorinated silane thin films with antiadhesive properties

Giulia Laghi[1], Domenico Franco[2], Vittorio Colombo[1,3,4,5], Guglielmo Guido Condorelli[6], Riccardo Gallerani[1], Salvatore Guglielmino[2], Romolo Laurita[1,3,8], Dario Morganti[9], Francesco Traina[9,10], Sabrina Conoci[2,9,11,12,13], Matteo Gherardi[1,4,5*]

---

[1] Department of Industrial Engineering, Alma Mater Studiorum - University of Bologna, 40136 Bologna, Italy

[2] Department of Chemical, Biological, Pharmaceutical and Environmental Sciences, University of Messina, 98166 Messina, Italy

[3] AlmaPlasma s.r.l., 40127 Bologna, Italy

[4] Interdepartmental Centre for Industrial Research Advanced Mechanical Engineering Applications and Materials Technology, Alma Mater Studiorum - University of Bologna, 40136 Bologna, Italy

[5] Interdepartmental Centre for Industrial Research Agrifood, Alma Mater Studiorum - University of Bologna, 40131 Bologna, Italy

[6] Department of Chemical Science, University of Catania, 95125 Catania, Italy

[7] Consorzio Interuniversitario di Scienze e Tecnologie dei Materiali (INSTM) UdR of Catania, 95125 Catania, Italy

[8] Interdepartmental Centre for Industrial Research Health Sciences and Technologies, Alma Mater Studiorum - University of Bologna, 40064 Ozzano dell'Emilia (BO), Italy

[9] IBMTech s.r.l., 95127 Catania, Italy

[10] Department of Biomedical and Neuromotor Sciences, Alma Mater Studiorum - University of Bologna, 40126 Bologna, Italy

[11] Department of Chemistry ''Giacomo Ciamician'', Alma Mater Studiorum – University of Bologna, 40126 Bologna, Italy

[12] LAB Sense Beyond Nano - URT Department of Sciences Physics and Technologies of Matter (DSFTM) CNR, 98166 Messina, Italy

[13] Istituto per la Microelettronica e Microsistemi, Consiglio Nazionale delle Ricerche (CNR-IMM), 95121 Catania, Italy.

*Correspondence
Matteo Gherardi
Department of Industrial Engineering, Alma Mater Studiorum - University of Bologna, 40136 Bologna, Italy
Email: matteo.gherardi4@unibo.it

Abstract

Finding proper strategies to control plasma polymerization processes is a crucial aspect to produce thin films with tailored characteristics. In this work, the validity of the Yasuda Parameter W/FM (W: discharge power and FM: precursor feed rate) as controlling parameter for a polymerization process assisted by an atmospheric pressure single electrode plasma jet and the aerosolized fluorinated silane precursor trimethoxy(3,3,3-trifluoropropyl)silane is demonstrated. The properties of thin films deposited under different W/FM values are discussed using attenuated total reflectance – Fourier transform infrared (ATR-FTIR) spectroscopy, X-ray photoelectron spectroscopy (XPS), water contact angle (WCA) measurements, and scanning electron microscopy (SEM). Results suggest the presence of two deposition domains as a function of W/FM (an energy-deficient and a monomer-deficient domains), each inducing coatings with different chemical and physical properties. Furthermore, coatings deposited under same W/FM values exhibit similar characteristics regardless of the power and feed rate values adopted. Considering the potential use of the deposited coatings to increase the antiadhesive properties of implantable medical devices, preliminary results on coatings antiadhesive activity against *P. aeruginosa* and *S. aureus* are presented.

Keywords: AP-PECVD, process control, Yasuda Parameter, fluorine-containing coatings, aerosol precursor

1 INTRODUCTION

Plasma polymerization is a versatile technique to produce a wide range of thin films on various substrates [1]–[3]. Plasma polymerized thin films exhibit unique characteristics compared to the conventionally polymerized ones, such as a higher degree of cross-linking, insolubility, thermal stability, and good adhesion to most substrates [4]–[7]. Therefore, these films are suitable for numerous industrial applications, including optics, electronics, and medical devices [8]–[10].

Despite plasma polymerization was traditionally performed at low pressure (10-100 Pa), atmospheric pressure plasma polymerization is receiving increasing attention due to the absence of expensive vacuum equipment and the possibility of in-line processing [11]–[14]. However, at atmospheric pressure the mean free path of reactive species is significatively shorter than at low pressure, thus resulting in a more complex gas chemistry [4], [15].

Whatever the pressure, researchers have always had a strong interest in controlling plasma polymerization processes by correlating the deposition parameters to the properties of the deposited thin films [16]. Originally, in the context of low pressure polymerization, Yasuda proposed the controlling parameter W/FM, later named Yasuda Parameter, which relates the discharge power (W) to the product of the precursor molar flow rate (F) and the precursor molecular weight (M) [17], [18].

This parameter represents an energy input per unit mass of precursor and is strictly connected to the precursor fragmentation process: low W/FM values result in a reduced fragmentation of the precursor molecules and consequently in a higher retention of precursor functional groups in the deposited thin films, while higher values lead to an intense fragmentation of the precursor molecules and thus to a loss of precursor functional groups in the films. The described behaviors correspond to different operating regions in plasma polymerization (power-deficient region and monomer-deficient region, respectively) which can be identified by plotting the thin film deposition rate as a function of W/FM [19].

More recently, Hegemann et al. further developed this idea offering a macroscopic description of plasma polymerization which implies a unifying dependence of the deposition rate per unit of monomer flow (R_m/F) to W/FM trough the quasi-Arrenhius expression:

$$\frac{R_m}{FM} = G exp\left(-\frac{E_a}{\frac{W}{FM}}\right) \quad (1)$$

where G is a reactor-depending geometrical factor related to the maximum conversion of the precursor into film growth and E_a the apparent activation energy required to initiate chemical reactions in the plasma zone [20]–[22].

W/FM was extensively used in low pressure plasma polymerization processes but over the years several research groups attempted to extend its application also to the atmospheric pressure case [1], [5], [8], [23]–[25]. Nonetheless, the validity of W/FM as a control parameter at atmospheric pressure has been questioned because, differently from low pressure processes, the precursor is typically highly diluted in an ionization gas which takes part in the mechanisms of energy transfer to the precursor molecules [16], [26].

For this reason, a methodology for measuring the energy absorbed per molecule in atmospheric pressure plasma polymerization processes have been developed and proposed as a more accurate alternative to the Yasuda Parameter [16], [27], [28]. Despite being validated for different families of precursors, this methodology is still limited to the context of planar dielectric barrier discharges (DBDs) and to vaporized precursors [29]–[35]. The choice of the authors to focus on this experimental configuration is certainly not accidental: DBDs are appealing for a wide range of industrial applications due to the easy formation of a stable discharge and their scalability [8], [36], while vaporized precursors are the most commonly used in plasma polymerization processes [37].

Nevertheless, the number of plasma sources of high industrial potential is much broader. For example, atmospheric pressure plasma jets are gaining interest since they are suitable for the coating of complex three-dimensional geometries and for the possibility to scale down the dimension of the spot treatment to the submillimeter range [38]–[40]. At the same time, as at atmospheric pressure the precursor can be injected into the discharge in liquid phase, aerosolized precursors are increasingly used because of the peculiar advantages respect to the vaporized ones, such as the lower complexity of the experimental setup and the less intense fragmentation of the precursor molecules in the discharge [37], [41]–[43].

For atmospheric pressure plasma polymerization processes which involve elements such as the above described, the validity of the Yasuda Parameter as a process control parameter should be demonstrated on a case-by-case basis. In this work, the use of W/FM as control parameter for a plasma polymerization process assisted by a single electrode plasma jet and an aerosolized precursor is investigated. The chemical and physical properties of the thin films are deposited under different W/FM values are characterized by means of attenuated total reflectance – Fourier transform infrared (ATR-FTIR) spectroscopy, X-ray photoelectron spectroscopy (XPS), water contact angle (WCA) measurements, and scanning electron microscopy (SEM).

A fluorinated silane precursor, trimethoxy(3,3,3-trifluoropropyl)silane, is selected for this work with the aim of depositing fluorine containing coatings suitable for antibacterial

applications. In fact, it is known that these coatings can exhibit antiadhesive properties, thus representing a potential strategy to contain the onset of severe infections associated with the formation of biofilm of implantable medical devices (e.g. prostheses). [44], [45] These infections typically result in huge implications both for the patients and for the National Health Service and current treatments consist in prolonged and high-dose antibiotic therapies that are often ineffective, due to the antibiotic-resistant nature of biofilms [46]; consequently, removal of the prosthesis is necessary to prevent the infection from becoming systemic, however exposing the patient to high risks. In this perspective, the development of antiadhesive surfaces for implantable medical devices is a high priority topic of research [47]–[50].

Considering the potentialities in the biomedical field of the plasma polymerization process explored in this work, preliminary biological results of the antiadhesive activity of the deposited coatings against *P. aeruginosa* and *S. aureus* are presented.

2 EXPERIMENTAL SECTION

2.1 Experimental setup

The experimental setup used in this work is schematically reported in Figure 1.

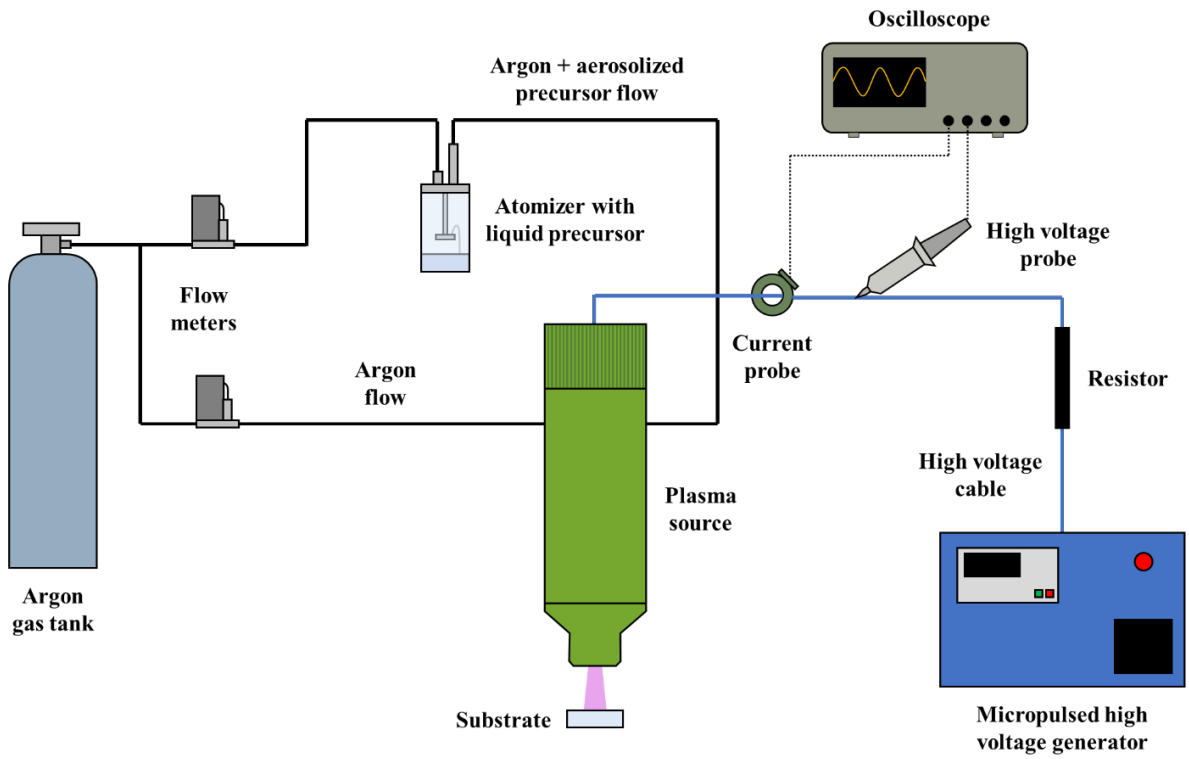

Figure 1: Schematical representation of the experimental setup

The employed plasma source is an atmospheric pressure single electrode plasma jet (AlmaJET, AlmaPlasma s.r.l.), whose detailed description can be found in [51]–[54]. An argon flow rate of 3 slpm was injected in the discharge region through the primary channel, while, simultaneously, an aerosolized precursor flow rate is introduced through the secondary channel. The liquid precursor used in this work is (3,3,3-trifluoropropyl)trimethoxysilane ($C_6H_{13}F_3O_3Si$, Sigma-Aldrich, ≥ 97.0%) and is characterized by three methoxy groups and a trifluoromethyl group, as shown in Figure 2.

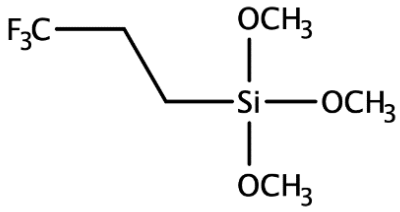

Figure 2: Precursor molecular structure

To the best of our knowledge, the only study dedicated to plasma polymerization of this precursor at atmospheric pressure was focused on the influence of several parameters (i.e. electrode-substrate gap distance, deposition time, and mode of deposition (static or dynamic)) on the overall deposition characteristics [55]. Hence, the role of W/FM as control parameter for processes involving this precursor is yet unexplored.

A single-jet atomizer (BLAM, CH Technologies) fed with an argon flow was used to aerosolize the liquid precursor. To calculate the effective precursor feed rate, the quantity of liquid precursor consumed within a defined time interval (15 min) was measured. The argon flow rates were controlled by digital mass flow controllers (EL-FLOW, Bronkhorst).

The stainless-steel single electrode of the plasma source was connected to a micropulsed high voltage generator (AlmaPulse, AlmaPlasma s.r.l.), operated at a fixed frequency of 12 kHz and at a variable peak voltage; a ballast resistor of 70 kΩ was added along the high voltage cable between the generator and the plasma source. Bilayer films (area: 1 cm x 1 cm, thickness: 0.3 mm), composed of polyethylene (PE, approximately 0.15 mm thick) and polyvinyl chloride (PVC, approximately 0.15 mm thick) foils, were used as substrates, and were rinsed for 2 minutes with ethanol (Sigma Aldrich, ≥ 99.8%) to remove contaminants and dried in air prior to deposition. The deposition was performed onto the PE layer and the distance between the electrode tip and the surface of the substrate under the plasma source was kept constant to 10 mm. The deposition time was fixed to 60 s.

Nine different combinations of peak voltage and precursor feed rate (covering the maximum operating range of the plasma jet source and the atomizer, respectively) were

analyzed. Each combination, associated to a letter from A to I, is reported in Table 1 along with the corresponding discharge power and W/FM value. Conditions from J to M, reported as well in Table 1, were investigated to study the properties of coatings deposited under identical W/FM values but obtained with different combinations of power discharge and precursor feed rate. The performed comparisons are the following: D-J, E-K, F-L, and H-M.

Deposition condition	**Peak voltage [kV]**	**Precursor feed rate [g/h]**	**Discharge power [W]**	**W/FM [MJ/kg]**
A	14	0.7	11.7 ± 0.6	60.2 ± 3.1
B	12	0.7	7.5 ± 0.4	38.6 ± 2.1
C	10	0.7	5.1 ± 0.3	26.2 ± 1.5
D	8	0.7	2.8 ± 0.4	14.4 ± 2.1
E	6	0.7	1.7 ± 0.2	8.7 ± 1.0
F	6	1.2	1.8 ± 0.1	5.4 ± 0.3
G	6	2.1	1.8 ± 0.1	3.1 ± 0.2
H	6	4.56	1.9 ± 0.2	1.5 ± 0.2
I	6	9.32	2.2 ± 0.1	0.8 ± 0.0
J	10	1.2	5.3 ± 0.4	15.9 ± 1.2
K	8	1.2	2.9 ± 0.1	8.7 ± 0.3
L	8	2.1	3.0 ± 0.2	5.1 ± 0.3
M	8	9.32	3.8 ± 0.2	1.5 ± 0.1

Table 1: Analyzed deposition conditions

To calculate the discharge power, the voltage (V) and the current (i) were measured by means of a high voltage probe (Tektronix P6015A) and a current probe (Pearson 6585), both located on the high voltage cable between the resistor and the plasma source. The corresponding waveforms were recorded using a digital oscilloscope (Tektronix DPO4034, 350 MHz, 2.5 GSa/s). As an example, Figure 3 shows voltage and current waveforms corresponding to a representative applied voltage period (deposition condition A).

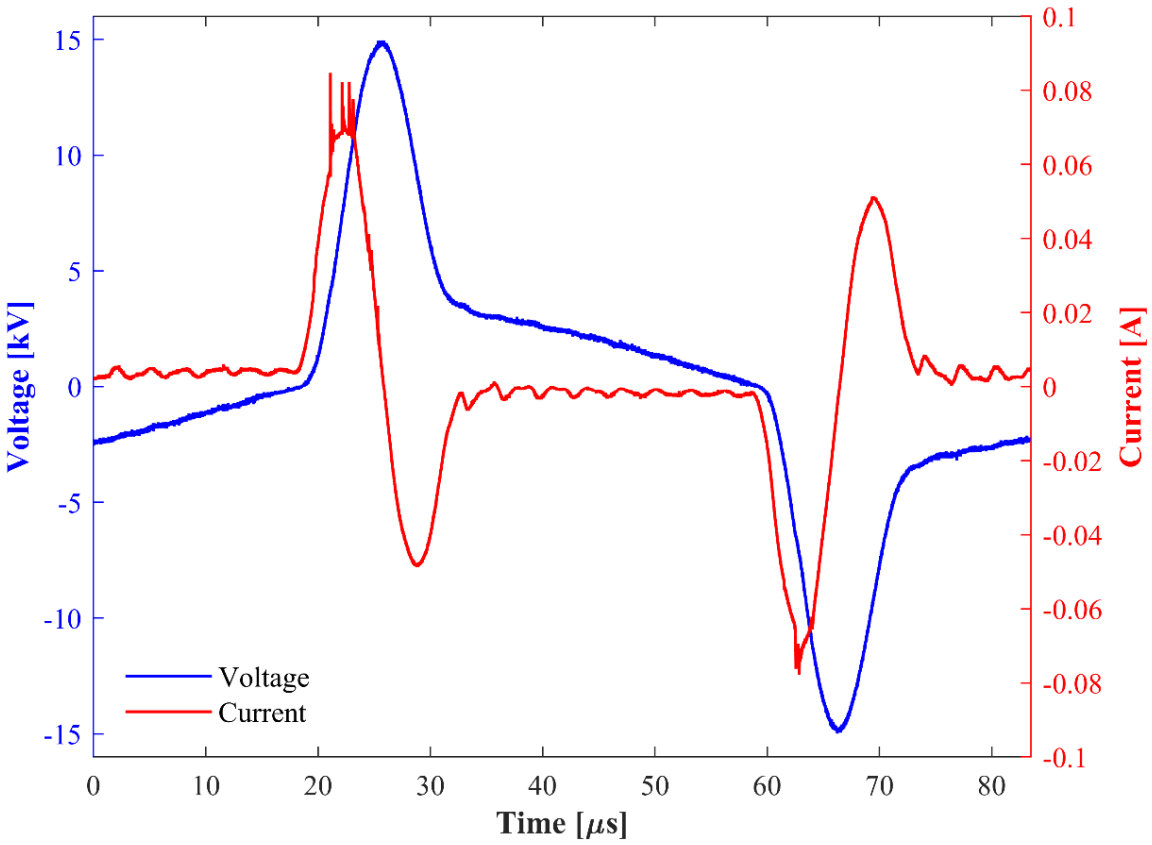

Figure 3: Voltage and current waveforms for deposition condition A

The average discharge power (P) dissipated over the applied voltage period (T) was calculated directly from measured voltage and current using the following formula:

$$P = \frac{1}{T}\int_0^T V(t)\, i(t)\, dt \quad (2)$$

To monitor the discharge power evolution during the treatment, the electrical characterization was performed at 0 s, 20 s, 40 s, and 60 s from the plasma ignition. For all the investigated conditions, the discharge power resulted constant in time, thus the representative discharge power value to be associated with the specific condition was calculated considering all the values obtained from the measurements performed during the treatment. Three replicates for each deposition condition were involved in the calculation (12 values in total), hence the results are shown as mean value ± standard deviation. The calculated discharge power was related to the precursor feed rate to calculate the corresponding W/FM values, which are presented as mean ± standard deviation as well.

2.2 Surface characterization of the deposited coatings

Fourier transform infrared (FTIR) measurements were performed to gather information on the chemical structure of the flat PE substrates before and after the deposition of the fluorinated silane coatings. The Agilent Cary 660 FTIR spectrometer was equipped with an attenuated total reflectance (ATR) sampling accessory, using a diamond crystal as internal reflection element and a beam set at 45°. Spectra were acquired in absorbance mode, from 4000 to 400 cm^{-1} with a resolution of 4 cm^{-1}; a total of 32 scans were recorded for each spectrum. The choice of PE as substrates facilitates the interpretation of ATR-FTIR coatings spectra since PE peaks appear in spectral regions other than those typically characteristic of silane coating peaks.

X-ray Photoelectron Spectroscopy (XPS) was used to study the chemical composition of PE substrates and of the deposited fluorinated silane coatings. Spectra were recorded with a PHI 5000 Versa Probe Instrument equipped with a monochromatic Al Kα X-ray source excited with a micro-focused electron beam. Analyses were carried out at 15 W on 150 μm area with a photo-electron take-off angle of 45°. The XPS binding energy (BE) scale was calibrated by centring the C 1s peak due to C-C, C-H hydrocarbon moieties of PE and "adventitious" carbon at 285.0 eV. [56]

Static water contact angle (WCA) measurements were carried out to evaluate the wettability of the deposited coatings and to compare it with that of the uncoated substrates. For the WCA measurements a drop shape analyzer (DSA30, KRUSS) was employed, depositing distilled water droplets (2 μl) on the substrates, and using the Young–Laplace method. For each deposition condition, 3 replicates were analyzed, performing 5 measurements for each replicate. The results are presented as mean values ± standard deviations.

Scanning electron microscopy (SEM) was used to investigate the thickness of the deposited coatings. To facilitate the break in liquid nitrogen, polypropylene foils (thickness 0.5 mm and diameter 2 cm) were chosen as substrates (after verifying that the deposited coatings possess identical chemical characteristics to coatings deposited on PE/PVC foils) and a pre-cut was performed in the back of the samples prior to the deposition treatment. To carry out more accurate thickness measurements, the deposition time was set to 120 s. The observations were carried out using a SEM (Phenom ProX, ThermoFisher Scientific) by applying an accelerating voltage of 10 kV. A sputter coater (SC7620, Quorum Technologies) was used to cover the coating surface with gold before SEM analysis.

2.3 Biological assay

For adhesion assay parameters, *P. aeruginosa* (ATCC 27853 strain, LGC Promochem, Milan, Italy) and *S. aureus* (ATCC2 9213 strain, LGC Promochem, Milan, Italy) were chosen as representative gram-negative and gram-positive bacterial strains. *P. aeruginosa* and *S. aureus* were cultured in Bertani Broth (LB, Sigma-Aldrich, Milan, Italy) and Tryptone Soya Broth (TSB, Sigma-Aldrich, Milan, Italy), respectively, and maintained in the respective medium added with 20% glycerol at -80 °C until they were used.

Adhesion activity tests were conducted according to the procedure described by Satriano et al. [57] with some modifications. Specifically, for each strain, an overnight culture was inoculated in fresh medium (dilution ratio 1:100) and incubated for 5 h at 37 °C under shaking at 150 rpm until an optical density. Bacteria, in the semi-exponential phase of growth, were washed twice in phosphate-buffered saline (PBS), then resuspended in PBS to obtain a turbidity equivalent (McFarland standard) of 0.5, corresponding about 2×10^8 bacteria/mL. Then bacterial solution was stained with SYTO9 green fluorescent nucleic acid stain (3.34 mM; Molecular Probes) for 15 minutes in the dark at 37 °C. 100 µL of stained bacterial suspension were put on the different treated surfaces and incubated in the humidified room for 2h.
Bacterial concentration (approximatively 2 x 10^8 bacteria/mL) and incubation times (2h) were chosen as the most suitable condition based on our previous experiences [58] and allowed to evidence the early stages of the adhesion process. In addition, since cell adhesion was evaluated in absence of nutrient to avoid any influence of the results by the components of the culture medium or cell proliferation during the incubation period, viability of both bacterial strains at different incubation times was preliminary monitored in PBS at room temperature, indicating a negligible reduction of viable counts after 2 hours (data not shown).

After the incubation, each sample was gently rinsed twice with sterile PBS and visualized under fluorescence microscopy by using Leica DMRE epifluorescence microscope (Leica Microsystems, Heerbrugg, Switzerland). From each sample, several fields of observation were captured and a quantitative evaluation of cells adhering onto the surface was performed using the Scion Image software (Windows version of NIH Image software) in the automated counting (single colour) image mode in terms of integrate density (IntDen), allowing to evaluate the cell coverage by the following equation:

$$IntDen = N \times (M - B) \tag{3}$$

where N is the number of pixels in the selection, M is the average grey value of the pixels, and B is the most common pixel value.

3 RESULTS

3.1 ATR-FTIR results

The ATR-FTIR spectra of PE substrates before and after the deposition under different W/FM values are shown in Figure 4.

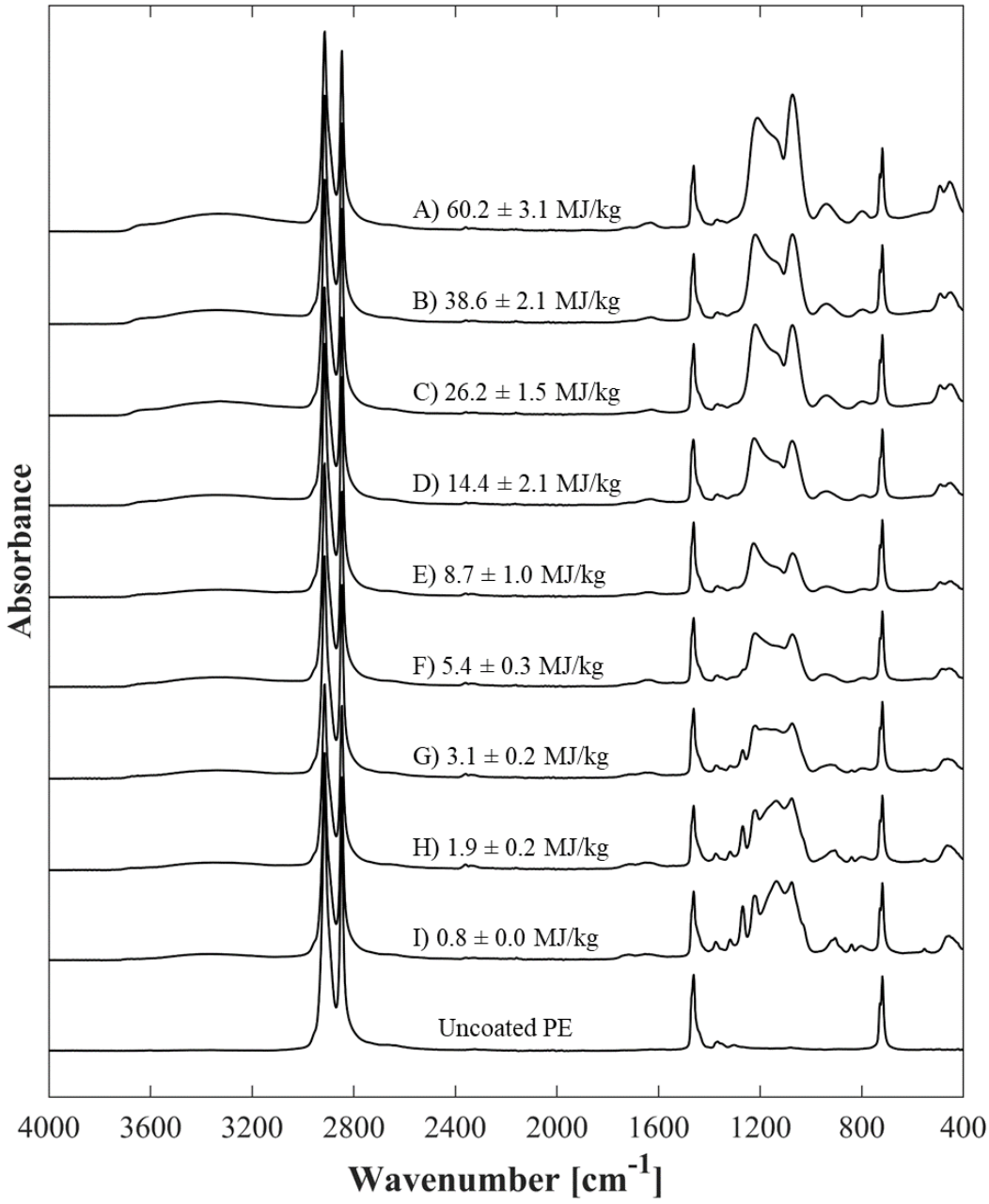

Figure 4: ATR-FTIR spectra of uncoated and coated PE substrates

The spectrum of uncoated PE exhibits two large absorption peaks at 2920 and 2852 cm^{-1} due to C-H asymmetric and symmetric stretching vibrations in CH_2, respectively. Furthermore, two smaller peaks can be observed at 1466 cm^{-1} and 723 cm^{-1}: the first corresponds to C-H deformation vibrations in $-(CH_2)_n-$, while the second one to C-C rocking vibrations in $-(CH_2)_n-$.[59], [60] The described peaks can be still detected in all the spectra related to coatings deposited under different W/FM values, suggesting that in no case the coating thickness exceeds

the penetration depth of the infrared beam (approximatively 550 nm in region 3000-2800 cm^{-1} and 1.1-2.3 μm in region 1500-700 cm^{-1}). For all the deposition conditions, bands corresponding to OH stretching vibrations at 3700-2800 cm^{-1} [61], [62] and C=C and C-O stretching vibrations at 1850-1650 cm^{-1} [63], [64] can be recognized. The main differences among coatings deposited under different W/FM values can be observed in the region 400-1400 cm^{-1}. A list of possible assignments of the peaks in this region is reported in Table 3.

Wavenumbers [cm^{-1}]	**Possible assignment**	**References**
1375	CH_3 deformation	[65], [66]
	CF_2 symmetric stretching	[67]
	CF stretching	[55]
1317	CF stretching	[55]
	CF_3 asymmetric stretching	[68]
1270	CF, CF_2, CF_3 stretching	[68]–[70]
	CH_3 deformation in Si-CH_3	[8], [71]
1220	CF_2 asymmetric stretching	[72]–[75]
1190	Si-O-Si asymmetric stretching (transverse optical, TO)	[76], [77]
1141	CF_2 asymmetric stretching	[67], [78]
1075	Si-O-Si asymmetric stretching (longitudinal optical, LO)	[36], [79], [80]
1040	C-O stretching	[81]
1029	CF or CF_3 stretching	[68], [69], [75]
930	Si-OH stretching	[36], [82], [83]
906	CH_2 rocking	[84]
880	Si-C stretching	[85]
840	CH rocking	[66]
	$Si(CH_3)_3$ stretching	[82]
800	Si-O-Si bending	[86], [87], [82]
	Si-O-Si stretching	[8], [79]
	Si-C stretching	[55]
	Si-$(CH_3)_2$ stretching	[87]
	CH_3 rocking	[8]
553	CF_2 bending	[67], [75]
495	CF_2 deformation	[88]
450	Si-O rocking	[89]

Table 2: Assignment of the peaks in the region 1400-4000 cm^{-1}

As W/FM decreases from condition A to condition E, no relevant differences in terms of peaks can be observed. All the spectra exhibit several peaks associated to silicon presence in the coating, such as the Si-O rocking at 450 cm^{-1}, the Si-O-Si bending or stretching at 800 cm^{-1}, the Si-O stretching at 900 cm^{-1}, the Si-OH stretching at 930 cm^{-1}, and the Si-O-Si asymmetric stretching at 1075 cm^{-1} (transverse optical, TO). Furthermore, peaks corresponding to CF_2

deformation at 495 cm^{-1} and to CF_2 asymmetric stretching at 1220 cm^{-1} can be recognized in all the spectra. Additional peaks, like the CF_2 asymmetric stretching at 1141 cm^{-1} and the Si-O-Si asymmetric stretching (longitudinal optical, LO) at 1190 cm^{-1}, can be clearly appreciated only by a proper deconvolution of the spectra. As an example, the deconvoluted spectrum (for wavenumbers comprised between 1000 and 1350 cm^{-1}) of coatings deposited in conditions A is reported in Figure 5a.

A different behavior can be observed in spectra from condition E to condition I, since a progressively higher fluorine and carbon content in the coatings can be detected as W/FM decreases. Fluorine-related peaks observed also in conditions A-E, like the one at 1141 cm^{-1}, become more pronounced, and the appearance of new peaks is registered at 553 cm^{-1}, 1030 cm^{-1}, 1270 cm^{-1}, 1316 cm^{-1} and 1370 cm^{-1} mainly attributed to CF_x (x=1,2,3), at 840 cm^{-1} and 906 cm^{-1} associated to CH_x (x=1,2,3) vibrations, at 880 cm^{-1} associated to Si-C stretching, and at 1040 cm^{-1} related to C-O stretching. The described behavior occurs along with a reduction of the contribution of the Si-O-Si related peaks at 450, 1075 and 1190 cm^{-1}. Figure 5b shows the deconvoluted spectrum of coatings deposited in condition I.

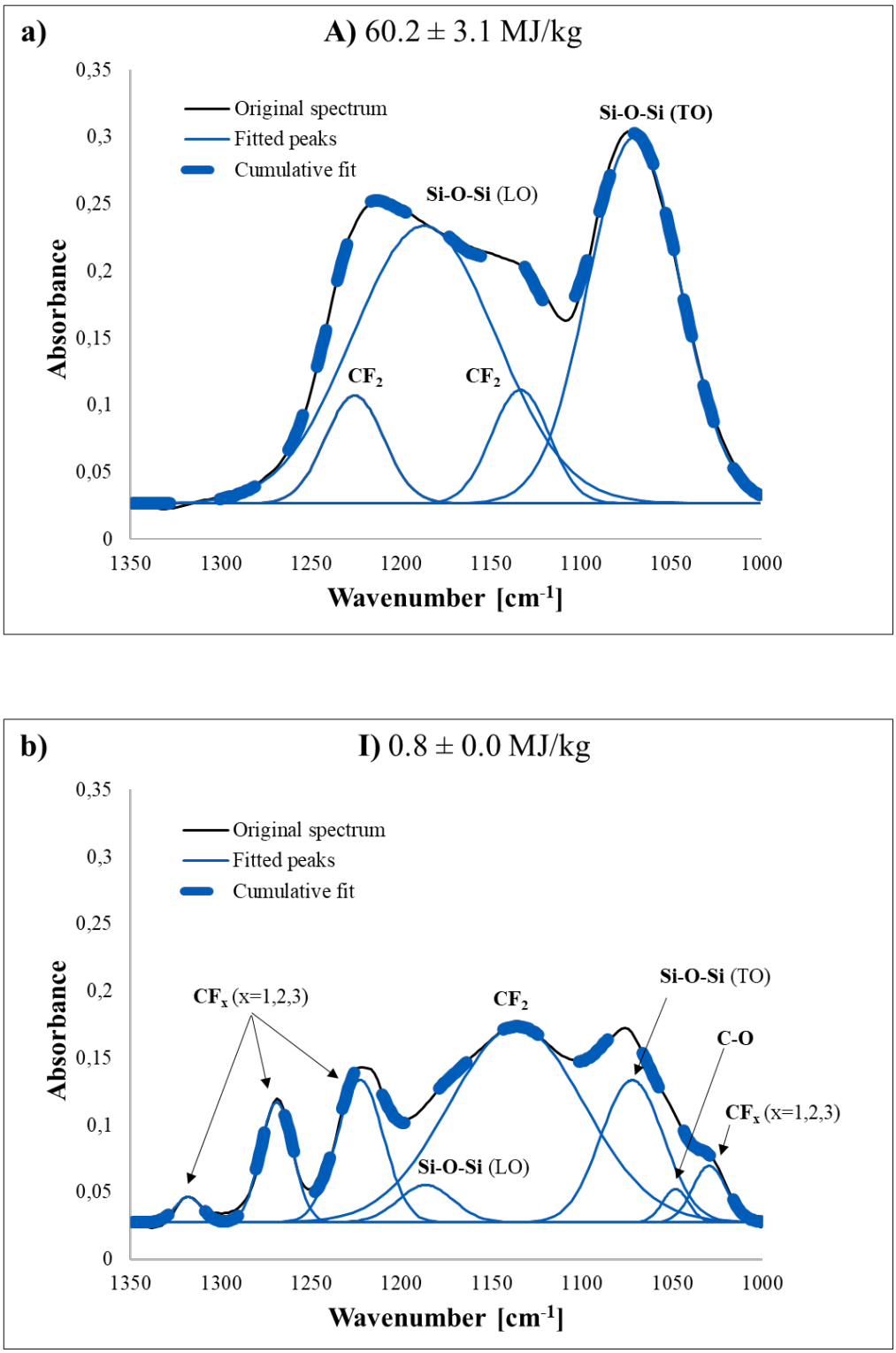

Figure 5: Deconvoluted spectra in conditions A (a) and I (b)

Since the deconvoluted spectra can provide quantitative information about the chemical composition of the coatings, the areas of two characteristic peaks present in all the investigated conditions, one related to the asymmetric stretching (LO) of Si-O-Si at 1190 cm^{-1} and one to CF_2 at 1141 cm^{-1}, were normalized respect to the total integrated area and plotted as a function of W/FM (Figure 6) to analyze the chemical behavior of the coatings while varying W/FM. The

ratio of the peaks and the total area remains almost constant for coatings deposited in conditions from A to E, while drastically changes between conditions E to I. More precisely, as W/FM decreases from E to I, the presence of the CF_2 asymmetric stretching increases at expenses of the Si-O-Si asymmetric stretching.

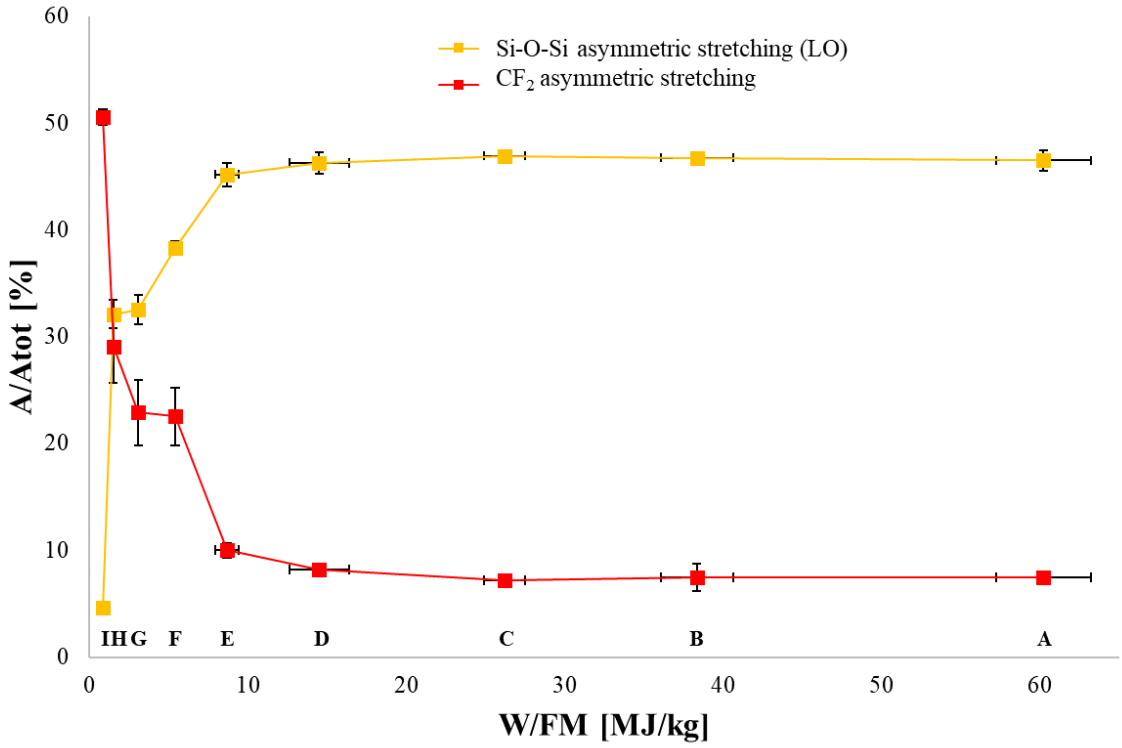

Figure 6: Ratio of the area of the peaks related to Si-O-Si asymmetric stretching (LO) and CF_2 asymmetric stretching and the total area as a function of W/FM

3.2 XPS results

C 1s, F 1s, O 1s and Si 2p XPS spectral regions of coatings obtained under different W/FM values are reported in Figure 7. In particular, only coatings deposited in conditions E (8.7 ± 1. MJ/kg), G (3.1 ± 0.2 MJ/kg), and I (0.8 ± 0.0 MJ/kg) were analyzed through XPS because no significant differences were observed in the ATR-FTIR spectra of samples obtained for W/FM values ranging from 60.2 to 8.7 MJ/kg (A-E conditions). The spectra of an uncoated PE substrate are added as references.

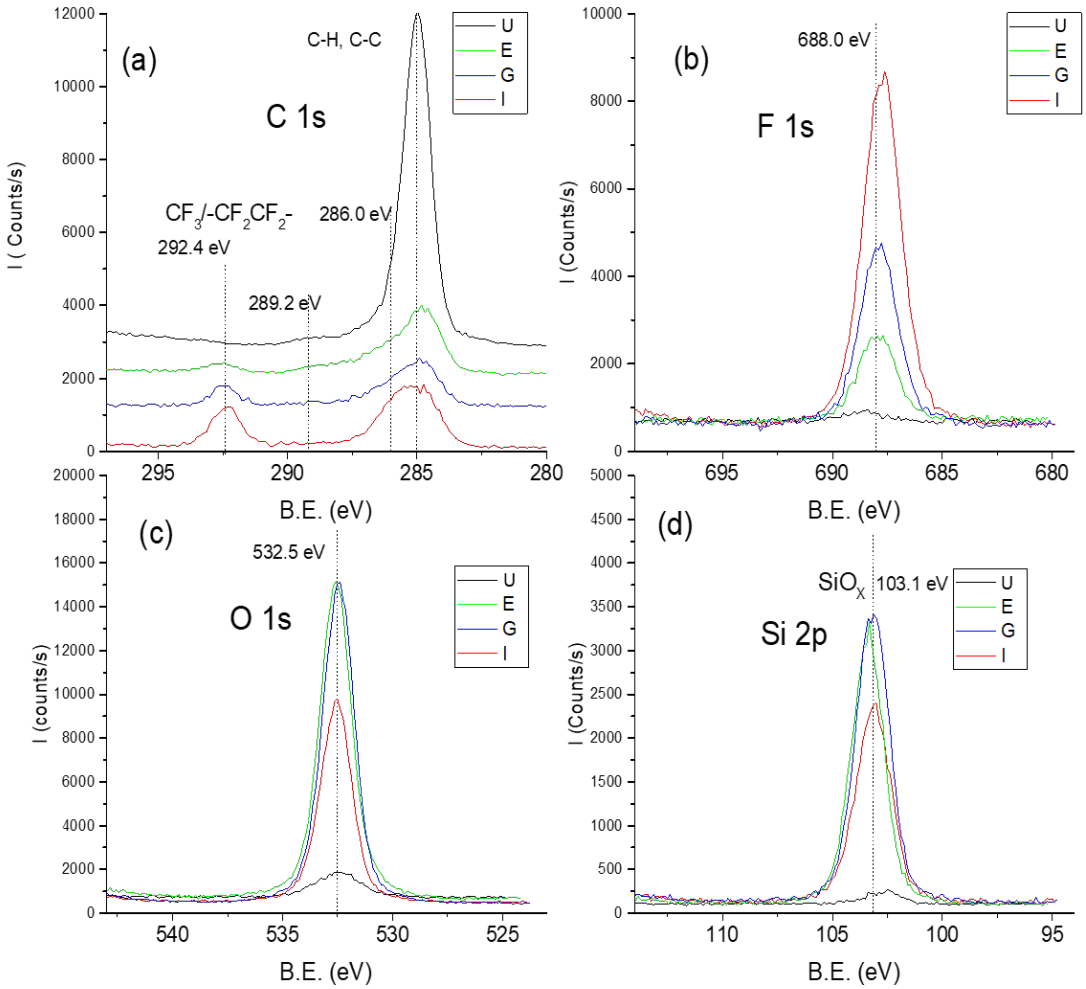

Figure 7: C 1s (a), F 1s (b), O 1s (c) and Si 2p (d) XPS spectral regions of the uncoated PE substrate (U) and of the coatings deposited in conditions E, G and I. C 1s spectra of the various samples are vertically translated for a better evaluation of the low intensity features.

C 1s spectrum (Fig 7a) of uncoated PE shows a main component at the Binding Energy (B.E.) of 285.0 eV due to -CH_2- of the polymer. [56], [90] The small band at about 289.2 eV due to carbon atoms of carboxylic groups [56], [91] is indication of a slight surface oxidation. After the coating deposition on the substrate, a new band at 292.4 eV whose intensity increases by decreasing the W/FM value can be observed. Band position is consistent with the presence of both CF_3 groups [90]–[92] and -CF_2-CF_2- chains [90], [92]. Besides the band at 292.4 eV, coatings show a low band at 289.2 eV, which decreases by decreasing W/FM until it is no longer observable for coatings obtained in condition I, and a shoulder at about 286.0 eV, which instead increases by decreasing W/FM. These two components can be due to a small amount of oxidized carbons (carboxylic and C-O groups, respectively), but contributions due to monofluorinated carbons (usually around 289-288 eV [92] and hydrocarbon atoms (CH_x) close to CF_x groups (usually around 286 eV [92] cannot be excluded. The increasing presence of

fluorinated groups by decreasing the W/FM ratio from E to I conditions is also confirmed by the atomic composition of the coatings obtained from XPS elemental analysis (Table 4) as well as by the spectrum of F 1s region (Figure 4b). Table 3 shows an evident increase of fluorine content by decreasing the W/FM ratio, which mirrors the increase of CF_3/-CF_2CF_2- groups. F 1s band consists of a single peak whose intensity increases moving from conditions E to I. The B.E is 688.0 eV for coatings deposited in condition E and decreases to 687.8 eV and 687.7 eV for conditions G and I, respectively. This B.E. shift suggests a progressive increase of CF_3 groups compared to CF_2 groups since F 1s B.E. is expected to be for CF_2 about 1.8 eV higher than CF_3 [92]. XPS elemental analysis (Table 3) shows that O and Si are also present in the coatings. Their concentrations slightly decrease reducing the W/FM ratio from E to G and strongly decrease for condition I. The B.E. positions of O1s (532.5 eV) and Si 2p (103.1 eV) peaks (Fig 4c and 4d) are consistent with the presence of SiO_x moieties [90], [93] whose amount is reduced for W/FM ratio below 3.1 MJ/kg.

Deposition condition	C_{tot} (CF_x)	O	F	Si
Uncoated PE	88.7 (0)	8.4	1.4	1.5
E	19.9 (1.4)	54.2	4.8	21.1
G	16.4 (3.4)	51.1	11.6	20.9
I	27.2 (7.2)	32.8	24.9	15.1

Table 3: XPS atomic concentration of uncoated PE substrates and coatings obtained under conditions E, G, and I.

3.3 WCA measurements

Water contact angles of thin films deposited under different W/FM values are reported in Figure 8. As W/FM decreases from condition A (60.2 ± 3.1 MJ/kg) to condition E (8.7 ± 1 MJ/kg), the contact angle remains constant around 58° degrees. At lower W/FM values, the contact angle gradually increases, reaching a maximum value of about 83°. The uncoated PE substrate exhibits a contact angle of 93.28° ± 4.84°, which is higher than all the measured angles for the deposited coating.

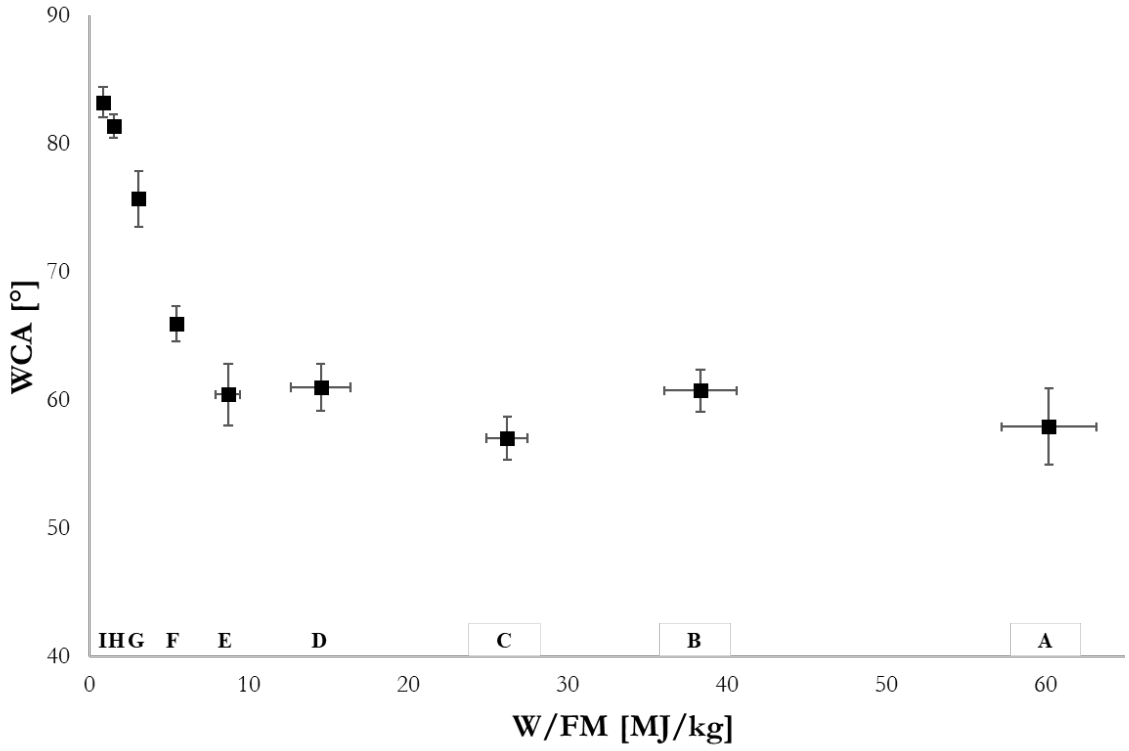

Figure 8: Water contact angles of thin films deposited under different W/FM values

3.4.2 SEM results: thickness

The deposition rate of coatings deposited under different W/FM values was calculated from SEM images by measuring the thickness of the cross section of samples broken in liquid nitrogen (Figure 9) and dividing it for the deposition time (2 minutes). The deposition rate, reported in Figure 10, is observed to decrease following a quasi-linear behaviour as W/FM decreases. Cross section images also highlight that, independently from the W/FM value, the structure of the coatings appears compact and non-porous.

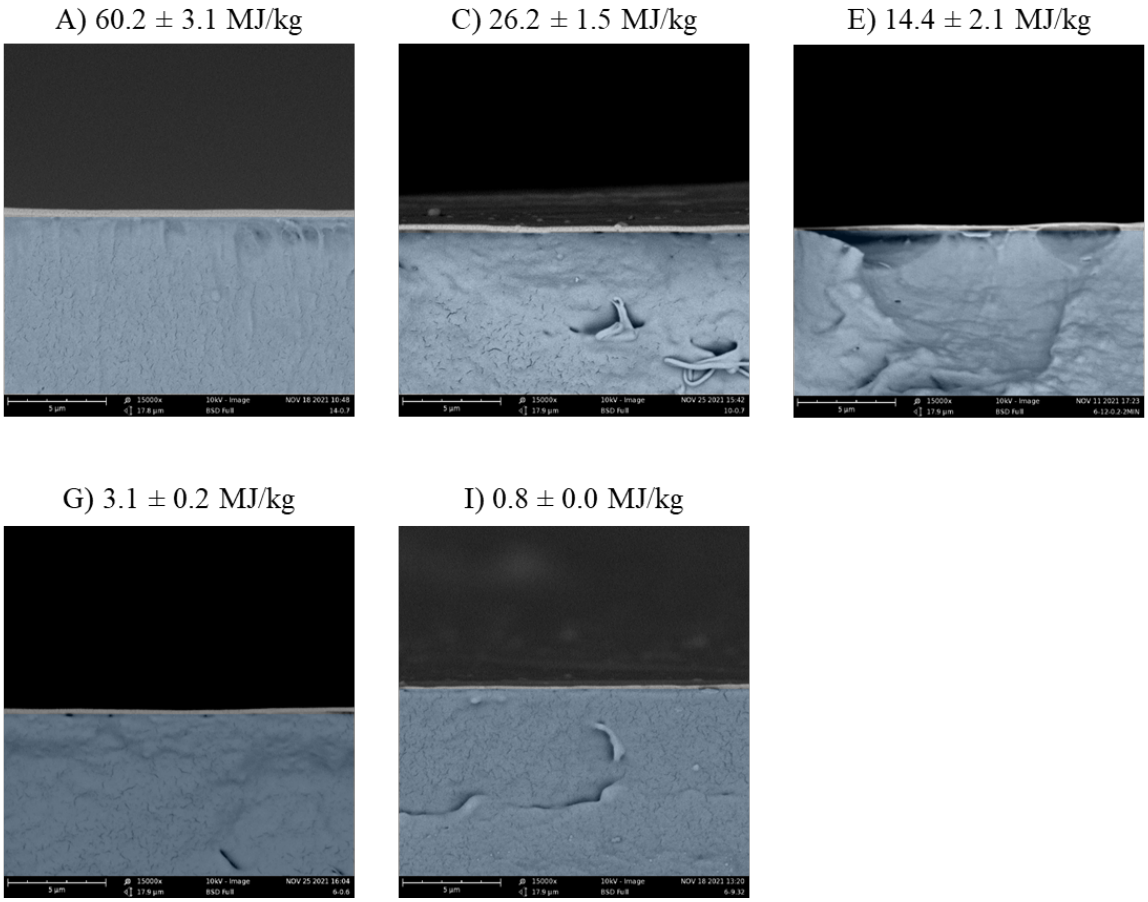

Figure 9: SEM images of cross-sections of thin films deposited under different W/FM values. To easily recognize the coating, the substrate is highlighted in light blue.

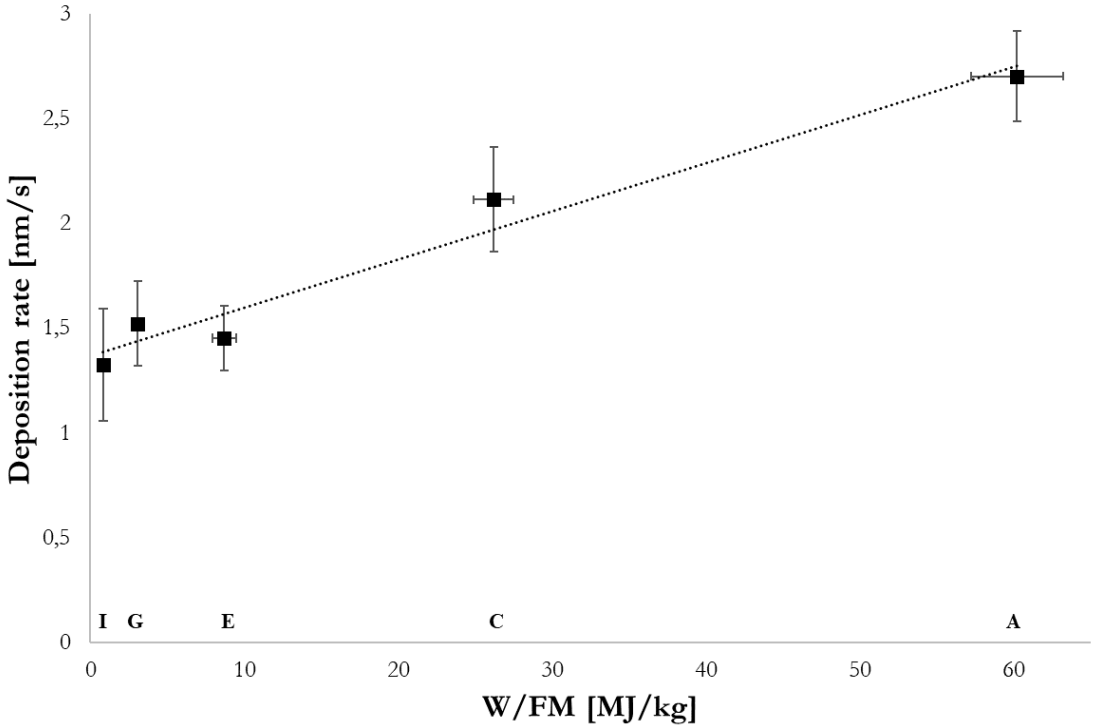

Figure 10: Coating deposition rate as a function of W/FM

3.4 Antiadhesive properties

The antibacterial activity of coatings deposited in condition E (8.7 ± 1.0 MJ/kg, representative of conditions ranging from A to E), G (3.1 ± 0.2 MJ/kg) and I (0.8 ± 0.0 MJ/kg) was assessed against *P. aeruginosa* and *S. aureus*. Adhesion patterns of both bacteria onto the uncoated PE and the coated surfaces are displayed in Figure 11. To easily associate the deposition condition to the investigated microorganism, subscripts P or S are added (e.g. E_P), representing *P. aeruginosa* and *S. aureus*, respectively.

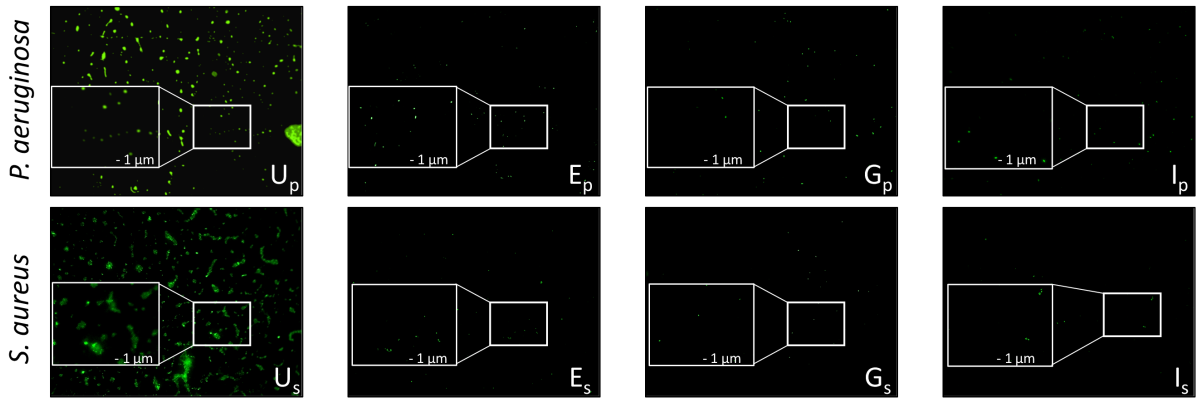

Figure 11: Fluorescent images of cells adhering on uncoated surface (U_P) and on surfaces coated in different deposition conditions: *P. aeruginosa* (first row) and *S. aureus* (second row). The inserts are magnifications of traced areas.

A visible reduction in the number of adhered bacteria can be observed on all the coated samples (Fig. 11E_P-I_P and 11E_S-Is) on the account of the antiadhesive properties of the deposited coatings. The quantitative evaluation of the cell adhesion, estimated by Scion Image Software, and the related percentages of covered area (% A) are showed in Table 5.

Deposition condition	***P. aeruginosa***		***S. aureus***	
	IntDen mean	% A	IntDen mean	% A
Uncoated PE	4009.7	2.95	6257.4	4.6
E	134.6	0.099	124.9	0.092
G	29.1	0.02	14.4	0.011
I	57.1	0.04	38.4	0.028

Table 5: Adhesion of *P. aeruginosa* and *S. aureus* cells on the uncoated and coated surfaces in terms of integrate density (IntDen) and related percentages of covered area (% A)

IntDen values of 4009.7 and 6257.4 can be deduced in uncoated samples for *P. aeruginosa* and for *S. aureus*, corresponding to covered areas (% A) of about 2.95% and 4.6%, respectively. When a coating deposited in condition E is present, IntDen values are significantly reduced: *P. aeruginosa* exhibits an IntDen value of 134.6, corresponding to 0.099% A, and *S. aureus* exhibits a 124.9 IntDen value, corresponding to 0.092% A. A further improvement in the antiadhesive properties can be observed decreasing the W/FM to condition G, showing IntDen 29.1 and 0.02% A for *P. aeruginosa* and IntDen 14.4 and 0.011% A for *S. aureus.* Finally, for coatings deposited in condition I (corresponding to the minimum W/FM), the percentage of cell surface coverage appears slightly increased, showing IntDen 57.1 and 0.04% A for *P. aeruginosa* and IntDen 38.4 and 0.028 % A for *S. aureus*.

By comparing the obtained percentages with those of the uncoated samples, a significant reduction (significance level of 99.9%, p-value < 0.001) is indicated by t-test for all the coated samples. *P. aeruginosa* adhesion rate is reduced by about 96.6% for E_P, 99.3% for G_P and 99.6% for I_P (Figure 12A), while *S. aureus* adhesion rate is reduced by 98% for G_s, 99.8% for G_S and 99.4% for I_S (Figure 12B). In addition, only coatings deposited in condition G result in a significant increase in the antiadhesive properties compared to the coatings deposited in condition E (significance level of 95%, with p-value of 0.0236 and 0.0369 for *P. aeruginosa* and *S. aureus,* respectively).

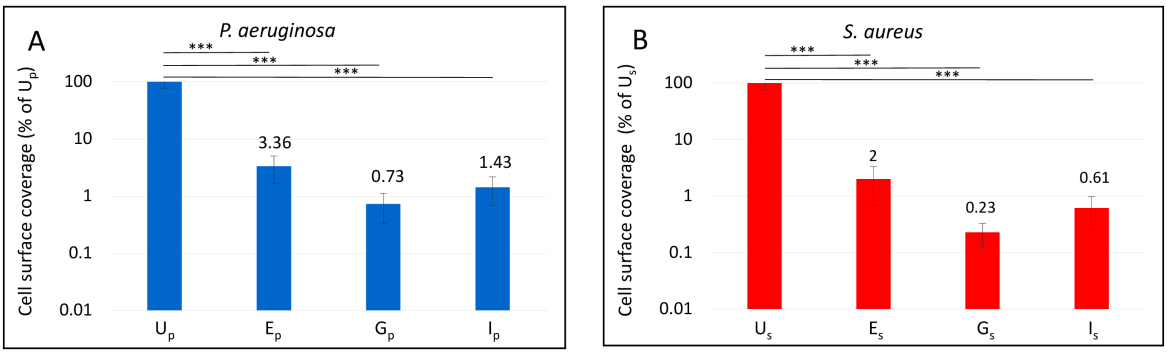

Figure 12: Percentage of cell surface coverage of coated samples vs uncoated samples for *P. aeruginosa* (A) and *S. aeurus* (B). Significance levels of 95% (*), 99% (**), 99.9% (***) are attributed for p-values lower than 0.05, 0.01 and 0.001 respectively. If not indicated, the deposition conditions do not show significant differences.

4 DISCUSSION

According to the results obtained with several surface characterization techniques, W/FM appears as a suitable control parameter for the process since its variation allows to work in two distinguished deposition regimes which lead to coatings with different chemical and physical characteristics. Indeed, ATR-FTIR spectra show the presence of two deposition regimes when varying W/FM: the regime associated to conditions from A (60.2 ± 3.1 MJ/kg) to E (8.7 ± 1 MJ/kg) and the one associated to conditions from E to I (0.83 ± 0.02 MJ/kg). Spectra of coatings deposited in the first regime do not change as a function of W/FM, exhibiting a predominant presence of peaks related to vibrations of the bonding Si-O-Si. Since the molecular structure of the starting precursor involves a central silicon atom surrounded by three oxygens and one carbon, the presence of bonding Si-O-Si suggests that the W/FM values in the first regime lead to an intense fragmentation of the precursor in the discharge. Nonetheless, even in these conditions of intense fragmentation, a minimum retention of precursor functional groups in the thin films is guaranteed, as confirmed by the presence of fluorine and carbon peaks. In the second regime, the chemical composition of the coatings drastically varies as W/FM decreases: new peaks associated to fluorine and carbon (in form of CF_x and CH_x, x = 1,2,3) appear at expenses of the vibrations of the bonding Si-O-Si. XPS analysis further supports these results, showing a progressive increase in the content of fluorine and carbon in the coatings as W/FM decreases. This behavior, observed also in other works in literature related to plasma polymerization processes at atmospheric pressure [8], [10], can be explained considering the lower values of W/FM in the second regime respect to the ones in the first regime: as the energy per precursor unit is reduced, the fragmentation of the precursor in the discharge becomes less intense and an increased presence of the functional groups of the precursor can be observed in the coating.

The existence of two deposition regimes can be clearly appreciated also by analyzing the behavior of the ratios of the areas of peaks related to the asymmetric stretching (TO) of Si-O-Si at 1190 cm^{-1} and of the one associated to one to CF_2 at 1141 cm^{-1} respect to the total integrated area (ATR-FTIR quantitative analysis) as a function of W/FM. As W/FM decreases from A to E, both the ratios stay constant, suggesting a similar chemical composition for the coatings deposited in those conditions, while they vary from E to I highlighting a major retention of characteristic functional groups in the coatings.

Water contact angle analysis provides a further confirmation of the presence of the two deposition regimes hypothesized based on ATR-FTIR and XPS analysis. Indeed, the wettability of the coating remains constant as W/FM decreases from condition A to condition E and then gradually decreases from E to I as W/FM decreases. The progressive decrease in the wettability of the coating is in agreement with the progressively higher presence in the coating of carbon and fluorine in form of alkyl and fluoroalkyl groups (CH_x and CF_x, with x = 1, 2, 3), which are known to increase the hydrophobicity degree of a surface [94].

The presence of two domains is further supported by SEM cross section analysis where the normalized deposition rate (obtained by dividing DR for the precursor feed rate FM) is considered (Figure 13).

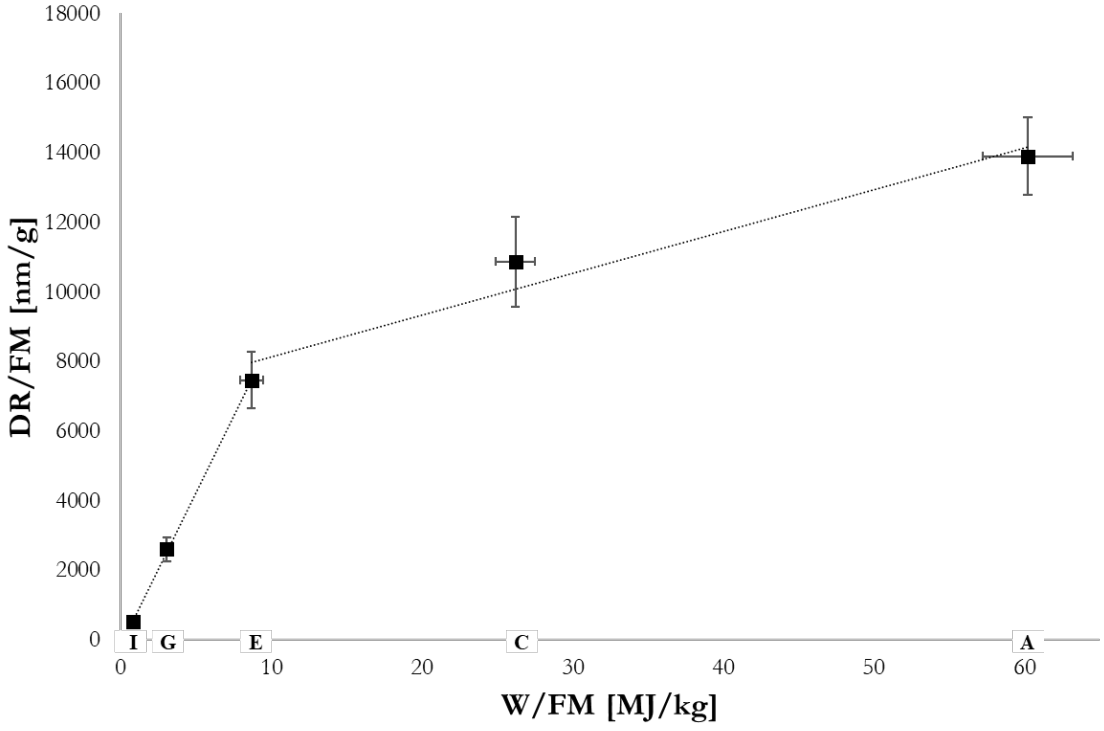

Figure 13: DR/FM as a function of W/FM

The behaviour of DR/FM as a function of W/FM has been discussed in detail in the work of Gilliam et al. [95], who investigated the plasma polymerization of fluorocarbon monomers in low pressure AF and RF discharges. In that work, the normalized deposition rate revealed two deposition domains for each monomer: the energy-deficient domain and the monomer-deficient domain. According to their discussion, the energy-deficient domain exists at low W/FM, in which the system contains excess of precursor, and the formation of depositing species is dependent on the energy input; in this domain, the normalized deposition rate increases linearly with W/FM. When a critical value of the Yasuda parameter $(W/FC)_c$ is reached, a further increase of energy does not create more depositing species and the normalized deposition rate remains constant; this region is called the monomer-deficient region, in which the precursor is analogous to a limiting reactant. In this work, a similar behaviour to the one obtained by Gilliam at al. can be observed and condition E can be recognized as the critical value of W/FM which marks the distinction in two deposition domains: the energy-deficient domain from I to E, where the slope of DR/FM as a function of W/FM is 880.85 [nm MJ g^{-1} kg^{-1}], and the monomer-deficient domain from E to A, with a slope of 119.97 [nm MJ g^{-1} kg^{-1}]. Correlating these results with what observed by means of all the other characterization techniques, in the energy-deficient domain the precursor undergoes to a limited fragmentation, resulting in high retention of fluorine and carbon content, while in the monomer-deficient region the energy excess results in intensive fragmentation and in a loss of characteristic functional groups.

According to the results presented and discussed so far, W/FM values from A to E lead to coatings with low retention of functional groups of the starting precursorand almost constant deposition rate, while W/FM from E to I to coatings with higher retention of functional groups of the starting precursor (such as CF_x and CH_x, x=1,2,3), increasing deposition rate. Nonetheless, it must be pointed out that conditions from A to E have been obtained using the same precursor feed rate and decreasing the discharge power, while conditions from E to I using the same discharge power and varying the precursor flow rate; in order to prove the controlling role of the Yasuda Parameter itself in the process, coatings deposited under the same W/FM parameter but calculated with a different combination of discharge power and precursor feed rate were compared. Quantitative ATR-FTIR analysis (Figure 14) and WCA analyses (Figure 15) highlight almost identical chemical composition and wettability for coatings deposited under same W/FM values. The obtained results suggest that W/FM might be a proper parameter for the control of a polymerization process assisted by an atmospheric pressure single electrode plasma jet and a fluorinated silane precursor.

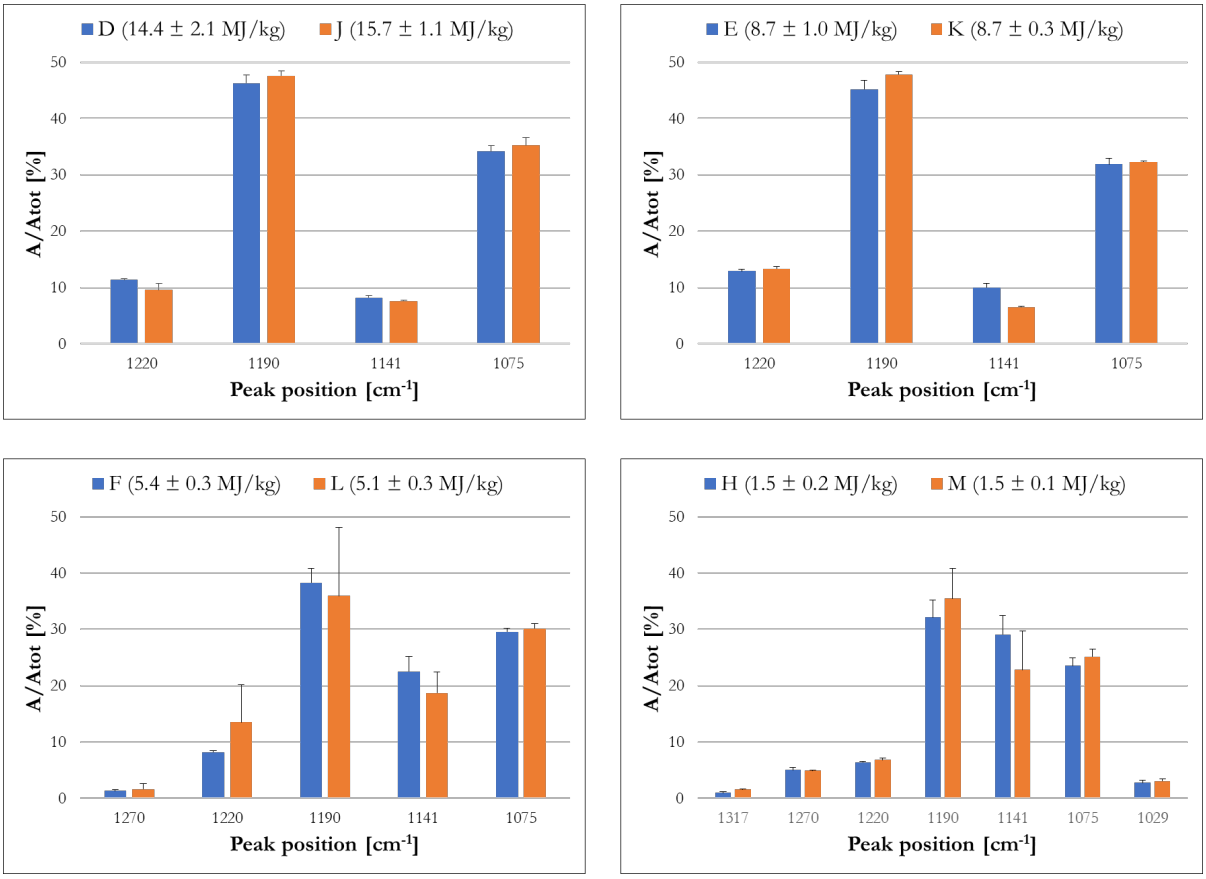

Figure 14: ratio of the area and the total area for peaks related to coating deposited under same W/FM values

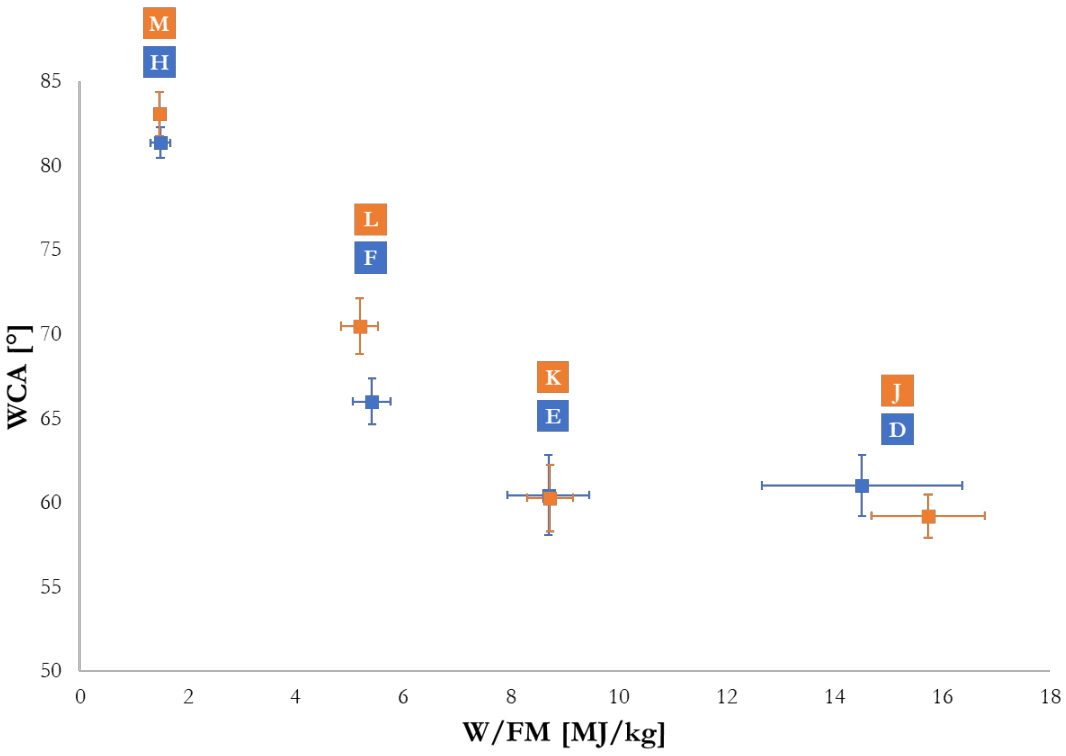

Figure 15: WCA of coatings deposited under same W/FM values

Prior to adhesion activity tests, morphological characteristics of coatings deposited under different W/FM values were analysed using Scanning Electron Microscopy (detailed results presented and discussed in supporting information). Considering the presence of fractures in conditions A and C (Figure 1 of supporting information), exclusively coatings deposited in condition E (characterized by same chemical composition of A and C), G and I were investigated in terms of antiadhesive properties.

Uncoated samples show a high number of adhered bacteria for both bacteria strains, mainly characterized by an adhesion pattern with island-like multi-layered cell aggregates and empty areas (Fig. $11U_P$ and $11sU_S$). According to the results, the surface covered by bacteria is higher for the case of *S. aureus,* as confirmed by IntDen values (4009.7 and 6257.4 for *P. aeruginosa* and *S. aureus,* respectively) and % A (2.95 and 4.6 for *P. aeruginosa* and *S. aureus,* respectively). However, all coated surfaces exhibit a significant reduction of initial bacterial attachment (reduction of 96.6% and 98% for *P. aeruginosa* and *S. aureus,* respectively). These findings can be attributed to the increased levels of fluorine and silicon compared to uncoated samples, as highlighted by XPS results. In fact, it is known that fluorine compounds have potential efficacy as antibacterial and anti-biofilm coating materials [44]. In this context, the highest antiadhesive effect is obtained in condition G, while a slight worsening is observed by further decreasing the W/FM value, namely condition I, even if the fluorine content is the highest (around 25%). As the contribution of the granular structure in condition I (Figure 1 of supporting information) on the antiadhesive activity of the surfaces cannot be excluded , further studies will be carried out to clarify the mechanisms underlying the interaction occurring between bacteria and coatings deposited under different W/FM conditions.

5 CONCLUSION

In this paper, an atmospheric pressure polymerization process assisted by an atmospheric pressure single electrode plasma jet and a fluorinated silane precursor is investigated. The aim of the work is to assess the validity of the Yasuda Parameter (W/FM) as a controlling parameter for the process since nowadays no alternative methodologies for the calculation of the energy absorbed by precursor molecules have been developed for plasma jets and aerosolized precursors. To reach this purpose, the characteristics of coatings deposited

under different W/FM values are analyzed using ATR-FTIR analysis, XPS analysis, WCA measurements, and SEM analysis.

ATR-FTIR and XPS results show the presence of two deposition domains as varying W/FM: one leading to coatings with a chemical composition that does not vary with W/FM, the other leading to coatings with a higher retention of functional groups of the starting precursors (such as CH_x and CF_x, x = 1,2,3) as W/FM progressively decreases. These findings are further confirmed by WCA measurements, which highlight a region of W/FM values where the wettability remains constant and one where the wettability decreases as W/FM decreases (probably due to the increased content of fluorine and carbon in the coating). The plot of the normalized deposition rate (DR/FM) as a function of W/FM reveals that the two deposition domains observed with the other characterization techniques can be associated with two deposition domains very well known in literature: the energy-deficient and the monomer-deficient domains. In addition to these evidences, the key role of the Yasuda Parameter in the process is further demonstrated since coatings deposited under the same W/FM exhibit similar properties, regardless of how W/FM is obtained.

As the interest to study this atmospheric pressure plasma polymerization process is related to the objective to create antiadhesive surfaces which can prevent the formation of biofilm on implantable medical devices, the antiadhesive activity of coatings deposited under different W/FM values (conditions E, G, I) is investigated against *P. aeruginosa* and *S. aureus*. The biological assay shows that the presence of a coating significatively improves the antiadhesive activity of the substrate and this is probably due to the presence of fluorine in the coating. Further decreasing the W/FM values until condition G contributes to increase the antiadhesive activity. Nonetheless, no further improvement can be seen for coatings deposited in condition I, which is the one with the highest fluorine content, suggesting that also other factors are probably involved in determining the antiadhesive properties of the surface.

ACKNOWLEDGMENTS

The authors thank the Bio-nanotech Research and Innovation Tower (BRIT) laboratory and the project: “Piano della ricerca di Ateneo 2020-22 linea 2” of the University of Catania for the PHI Versa Probe XPS facility.

AUTHOR CONTRIBUTIONS

FINANCIAL DISCLOSURE

CONFLICT OF INTEREST

The Authors declare no conflict of interest.

DATA AVAILABILITY STATEMENT

REFERENCES

[1] A. Kakaroglou *et al.*, "Deposition and characterisation of plasma polymerised allyl methacrylate based coatings," *Plasma Process. Polym.*, vol. 9, no. 8, pp. 799–807, 2012, doi: 10.1002/ppap.201100162.

[2] P. Cools, N. De Geyter, E. Vanderleyden, F. Barberis, P. Dubruel, and R. Morent, "Adhesion improvement at the PMMA bone cement-titanium implant interface using methyl methacrylate atmospheric pressure plasma polymerization," *Surf. Coatings Technol.*, vol. 294, pp. 201–209, 2016, doi: 10.1016/j.surfcoat.2016.03.054.

[3] S. Van Vrekhem, R. Morent, and N. De Geyter, "Deposition of a PMMA coating with an atmospheric pressure plasma jet," *J. Coatings Technol. Res.*, vol. 15, no. 4, pp. 679–690, 2018, doi: 10.1007/s11998-018-0049-4.

[4] N. De Geyter *et al.*, "Deposition of polymethyl methacrylate on polypropylene substrates using an atmospheric pressure dielectric barrier discharge," *Prog. Org. Coatings*, vol. 64, no. 2–3, pp. 230–237, 2009, doi: 10.1016/j.porgcoat.2008.07.029.

[5] M. Asandulesa, I. Topala, V. Pohoata, and N. Dumitrascu, "Influence of operational parameters on plasma polymerization process at atmospheric pressure," *J. Appl. Phys.*, vol. 108, no. 9, 2010, doi: 10.1063/1.3506528.

[6] J. Petersen *et al.*, "Atmospheric plasma deposition process: A versatile tool for the design of tunable siloxanes-based plasma polymer films," *Plasma Process. Polym.*, vol. 8, no. 10, pp. 895–903, 2011, doi: 10.1002/ppap.201100022.

[7] K. N. Pandiyaraj *et al.*, "Influence of operating parameters on development of polyethylene oxide-like coatings on the surfaces of polypropylene films by atmospheric pressure cold plasma jet-assisted polymerization to enhance their antifouling properties," *J. Phys. Chem. Solids*, vol. 123, no. June, pp. 76–86, 2018, doi: 10.1016/j.jpcs.2018.06.007.

[8] R. Morent *et al.*, "Plasma-polymerization of HMDSO using an atmospheric pressure

dielectric barrier discharge," *Plasma Process. Polym.*, vol. 6, no. SUPPL. 1, pp. 537–542, 2009, doi: 10.1002/ppap.200931101.

[9] P. E. C. Tan, C. L. S. Mahinay, I. B. Culaba, O. K. M. Streeter, and M. R. A. Hilario, "Plasma polymerization of styrene using an argon-fed atmospheric pressure plasma jet," *J. Vac. Sci. Technol. B*, vol. 36, no. 4, p. 04I102, 2018, doi: 10.1116/1.5030840.

[10] M. A. Gilliam, S. A. Farhat, G. E. Garner, B. P. Stubbs, and B. B. Peterson, "Characterization of the deposition behavior and changes in bonding structures of hexamethyldisiloxane and decamethylcyclopentasiloxane atmospheric plasma-deposited films*," *Plasma Process. Polym.*, vol. 16, no. 7, 2019, doi: 10.1002/ppap.201900024.

[11] S. Starostine, E. Aldea, H. de Vries, M. Creatore, and M. C. M. van de Sanden, "Atmospheric pressure barrier discharge deposition of silica-like films on polymeric substrates," *Plasma Process. Polym.*, vol. 4, no. SUPPL.1, pp. 440–444, 2007, doi: 10.1002/ppap.200731203.

[12] J. Pulpytel, V. Kumar, P. Peng, V. Micheli, N. Laidani, and F. Arefi-Khonsari, "Deposition of organosilicon coatings by a non-equilibrium atmospheric pressure plasma jet: Design, analysis and macroscopic scaling law of the process," *Plasma Process. Polym.*, vol. 8, no. 7, pp. 664–675, 2011, doi: 10.1002/ppap.201000121.

[13] K. N. Pandiyaraj *et al.*, "Development of phosphor containing functional coatings via cold atmospheric pressure plasma jet - Study of various operating parameters," *Appl. Surf. Sci.*, vol. 488, no. May, pp. 343–350, 2019, doi: 10.1016/j.apsusc.2019.05.089.

[14] H. J. Jang, E. Y. Jung, T. Parsons, H. Tae, and C. Park, "A Review of Plasma Synthesis Methods for Polymer Films and Nanoparticles under Atmospheric Pressure Conditions," 2021.

[15] Q. Chen *et al.*, "Atmospheric pressure dielectric barrier discharge synthesis of morphology-controllable TiO2 films with enhanced photocatalytic activity," *Thin Solid Films*, vol. 664, no. July, pp. 90–99, 2018, doi: 10.1016/j.tsf.2018.08.025.

[16] B. Nisol, H. Gagnon, S. Lerouge, and M. R. Wertheimer, "Energy of Reactions in Atmospheric-Pressure Plasma Polymerization with Inert Carrier Gas," *Plasma Process. Polym.*, vol. 13, no. 3, pp. 366–374, 2016, doi: 10.1002/ppap.201500068.

[17] H. Yasuda and T. Hirotsu, "Critical Evaluation of Conditions of Plasma Polymerization.," *J Polym Sci Polym Chem Ed*, vol. 16, no. 4, pp. 743–759, 1978, doi: 10.1002/pol.1978.170160403.

[18] H. Yasuda, "Glow Discharge Polymerization.," *J. Polym. Sci. Macromol. Rev.*, vol. 16, no. 198 1, pp. 199–293, 1981, doi: 10.1002/pol.1981.230160104.

[19] H. Yasuda, *PLASM A POLYMERIZATIO N*. 1985.

[20] D. Hegemann, M. M. Hossain, E. Körner, and D. J. Balazs, "Macroscopic description of plasma polymerization," *Plasma Process. Polym.*, vol. 4, no. 3, pp. 229–238, 2007, doi: 10.1002/ppap.200600169.

[21] D. Hegemann, E. Körner, and S. Guimond, "Plasma polymerization of acrylic acid revisited," *Plasma Process. Polym.*, vol. 6, no. 4, pp. 246–254, 2009, doi: 10.1002/ppap.200800089.

[22] D. Hegemann, "Macroscopic investigation of reaction rates yielding plasma polymer deposition," *J. Phys. D. Appl. Phys.*, vol. 46, no. 20, 2013, doi: 10.1088/0022-3727/46/20/205204.

[23] M. Bashir, J. M. Rees, and W. B. Zimmerman, "Plasma polymerization in a microcapillary using an atmospheric pressure dielectric barrier discharge," *Surf. Coatings Technol.*, vol. 234, pp. 82–91, 2013, doi: 10.1016/j.surfcoat.2013.01.041.

[24] J. Petersen *et al.*, "Nano-ordered thin films achieved by soft atmospheric plasma polymerization," *RSC Adv.*, vol. 3, no. 13, pp. 4416–4424, 2013, doi: 10.1039/c2ra21833j.

[25] A. Kakaroglou *et al.*, "Evaluation of the Yasuda parameter for the atmospheric plasma deposition of allyl methacrylate," *RSC Adv.*, vol. 5, no. 35, pp. 27449–27457, 2015, doi: 10.1039/c5ra02684a.

[26] G. Wulf, B. Mayer, and U. Lommatzsch, "Plasma Co-Polymerization of HMDSO and Limonene with an Atmospheric Pressure Plasma Jet," *Plasma*, vol. 5, no. 1, pp. 44–59, 2022, doi: 10.3390/plasma5010004.

[27] M. Archambault-Caron, H. Gagnon, B. Nisol, K. Piyakis, and M. R. Wertheimer, "Precise energy and temperature measurements in dielectric barrier discharges at atmospheric pressure," *Plasma Sources Sci. Technol.*, vol. 24, no. 4, 2015, doi: 10.1088/0963-0252/24/4/045004.

[28] S. Watson, B. Nisol, S. Lerouge, and M. R. Wertheimer, "Energetics of Molecular Excitation, Fragmentation, and Polymerization in a Dielectric Barrier Discharge with Argon Carrier Gas," *Langmuir*, vol. 31, no. 37, pp. 10125–10129, 2015, doi: 10.1021/acs.langmuir.5b02794.

[29] B. Nisol, S. Watson, S. Lerouge, and M. R. Wertheimer, "Energetics of Reactions in a Dielectric Barrier Discharge with Argon Carrier Gas: II Mixtures with Different Molecules," *Plasma Process. Polym.*, vol. 13, no. 5, pp. 557–564, 2016, doi: 10.1002/ppap.201500161.

[30] B. Nisol, S. Watson, S. Lerouge, and M. R. Wertheimer, “Energetics of Reactions in a Dielectric Barrier Discharge with Argon Carrier Gas: III Esters,” *Plasma Process. Polym.*, vol. 13, no. 9, pp. 900–907, 2016, doi: 10.1002/ppap.201600003.

[31] B. Nisol, S. Watson, S. Lerouge, and M. R. Wertheimer, “Energetics of reactions in a dielectric barrier discharge with argon carrier gas: IV ethyl lactate,” *Plasma Process. Polym.*, vol. 13, no. 10, pp. 965–969, 2016, doi: 10.1002/ppap.201600099.

[32] B. Nisol, S. Watson, S. Lerouge, and M. R. Wertheimer, “Energetics of reactions in a dielectric barrier discharge with argon carrier gas: V hydrocarbons,” *Plasma Process. Polym.*, vol. 14, no. 8, pp. 1–9, 2017, doi: 10.1002/ppap.201600191.

[33] B. Nisol, S. Watson, A. Meunier, D. Juncker, S. Lerouge, and M. R. Wertheimer, “Energetics of reactions in a dielectric barrier discharge with argon carrier gas: VI PEG-like coatings,” *Plasma Process. Polym.*, vol. 15, no. 3, pp. 1–10, 2018, doi: 10.1002/ppap.201700132.

[34] J. Mertens, S. Watson, B. Nisol, M. R. Wertheimer, and F. Reniers, “Energetics of reactions in a dielectric barrier discharge with argon carrier gas: VII anhydrides,” *Plasma Process. Polym.*, vol. 16, no. 5, pp. 1–7, 2019, doi: 10.1002/ppap.201800186.

[35] S. Watson, B. Nisol, and M. R. Wertheimer, “Energetics of reactions in a dielectric barrier discharge with argon carrier gas: VIII hydrofluoromethanes,” *Plasma Process. Polym.*, vol. 17, no. 6, pp. 1–13, 2020, doi: 10.1002/ppap.201900125.

[36] S. A. Starostin, M. Creatore, J. B. Bouwstra, M. C. M. Van De Sanden, and H. W. De Vries, “Towards roll-to-roll deposition of high quality moisture barrier films on polymers by atmospheric pressure plasma assisted process,” *Plasma Process. Polym.*, vol. 12, no. 6, pp. 545–554, 2015, doi: 10.1002/ppap.201400194.

[37] F. Massines, C. Sarra-Bournet, F. Fanelli, N. Naudé, and N. Gherardi, “Atmospheric pressure low temperature direct plasma technology: Status and challenges for thin film deposition,” *Plasma Process. Polym.*, vol. 9, no. 11–12, pp. 1041–1073, 2012, doi: 10.1002/ppap.201200029.

[38] J. Winter, R. Brandenburg, and K. D. Weltmann, “Atmospheric pressure plasma jets: An overview of devices and new directions,” *Plasma Sources Sci. Technol.*, vol. 24, no. 6, 2015, doi: 10.1088/0963-0252/24/6/064001.

[39] P. Scopece, A. J. Viaro, R. Sulcis, I. Kulyk, A. Patelli, and M. Guglielmi, “SiOx-based gas barrier coatings for polymer substrates by atmospheric pressure plasma jet deposition,” *Plasma Process. Polym.*, vol. 6, no. SUPPL. 1, pp. 705–710, 2009, doi: 10.1002/ppap.200931707.

[40] A. Liguori *et al.*, "Deposition of Plasma-Polymerized Polyacrylic Acid Coatings by a Non-Equilibrium Atmospheric Pressure Nanopulsed Plasma Jet," *Plasma Process. Polym.*, vol. 13, no. 3, pp. 375–386, 2016, doi: 10.1002/ppap.201500080.

[41] B. Nisol, C. Poleunis, P. Bertrand, and F. Reniers, "Poly(ethylene glycol) films deposited by atmospheric pressure plasma liquid deposition and atmospheric pressure plasma-enhanced chemical vapour deposition: Process, chemical composition analysis and biocompatibility," *Plasma Process. Polym.*, vol. 7, no. 8, pp. 715–725, 2010, doi: 10.1002/ppap.201000023.

[42] D. Merche, N. Vandencasteele, and F. Reniers, "Atmospheric plasmas for thin film deposition: A critical review," *Thin Solid Films*, vol. 520, no. 13, pp. 4219–4236, 2012, doi: 10.1016/j.tsf.2012.01.026.

[43] F. Palumbo, C. Lo Porto, F. Fracassi, and P. Favia, "Recent Advancements in the Use of Aerosol-Assisted Atmospheric Pressure Plasma Deposition," *Coatings*, vol. 10, p. 440, 2020, doi: 10.3390/ma13132931.

[44] Q. Bao *et al.*, "Antibacterial and anti-biofilm efficacy of fluoropolymer coating by a 2,3,5,6-tetrafluoro-p-phenylenedimethanol structure," *Colloids Surfaces B Biointerfaces*, vol. 151, pp. 363–371, 2017, doi: 10.1016/j.colsurfb.2016.12.020.

[45] S. Parsaei, J. Keeney, and J. Marschall, *Infections of Prosthetic Joints and Related Problems*, Fourth Edi. Elsevier Ltd, 2017.

[46] Z. Khatoon, C. D. McTiernan, E. J. Suuronen, T. F. Mah, and E. I. Alarcon, "Bacterial biofilm formation on implantable devices and approaches to its treatment and prevention," *Heliyon*, vol. 4, no. 12, p. e01067, 2018, doi: 10.1016/j.heliyon.2018.e01067.

[47] A. Trampuz and W. Zimmerli, "Prosthetic joint infections: Update in diagnosis and treatment," *Swiss Med. Wkly.*, vol. 135, no. 17–18, pp. 243–251, 2005, doi: 2005/17/smw-10934.

[48] R. D. Monds and G. A. O'Toole, "The developmental model of microbial biofilms: ten years of a paradigm up for review," *Trends Microbiol.*, vol. 17, no. 2, pp. 73–87, 2009, doi: 10.1016/j.tim.2008.11.001.

[49] J. Fu *et al.*, "Strategies for Interfering With Bacterial Early Stage Biofilms," *Front. Microbiol.*, vol. 12, no. June, pp. 1–15, 2021, doi: 10.3389/fmicb.2021.675843.

[50] A. Ghimire and J. Song, "Anti-Periprosthetic Infection Strategies: From Implant Surface Topographical Engineering to Smart Drug-Releasing Coatings," *ACS Appl. Mater. Interfaces*, vol. 13, no. 18, pp. 20921–20937, 2021, doi: 10.1021/acsami.1c01389.

[51] F. Barletta, A. Liguori, C. Leys, V. Colombo, M. Gherardi, and A. Nikiforov, “Novel method for NH-rich coatings engineering by means of aerosol assisted atmospheric pressure plasma deposition,” *Mater. Lett.*, vol. 214, pp. 76–79, 2018, doi: 10.1016/j.matlet.2017.11.116.

[52] F. Barletta and A. Nikiforov, “Insights into plasma - assisted polymerization at atmospheric pressure by spectroscopic diagnostics,” *Plasma Process. Polym.*, vol. 17, no. September, pp. 1–15, 2019, doi: 10.1002/ppap.201900174.

[53] F. Barletta, C. Leys, M. Gherardi, R. Snyders, and A. Nikiforov, “Studying the plasma - assisted polymerization at atmospheric pressure in Ar / TEOS by active laser diagnostics,” no. August 2020, pp. 1–15, 2021, doi: 10.1002/ppap.202000149.

[54] H. Malekzad, T. Gallingani, F. Barletta, M. Gherardi, V. Colombo, and D. Duday, “Single - step deposition of hexamethyldisiloxane surface gradient coatings with a high amplitude of water contact angles over a polyethylene foil,” *Plasma Process. Polym.*, vol. 18, no. August 2020, 2021, doi: 10.1002/ppap.202000044.

[55] J. H. Yim, V. Rodriguez-santiago, A. A. Williams, T. Gougousi, D. D. Pappas, and J. K. Hirvonen, “Atmospheric pressure plasma enhanced chemical vapor deposition of hydrophobic coatings using fl uorine-based liquid precursors,” *Surf. Coat. Technol.*, vol. 234, pp. 21–32, 2013, doi: 10.1016/j.surfcoat.2013.03.028.

[56] D. Briggs and G. Beamson, “Primary and Secondary Oxygen-Induced C1s Binding Energy Shifts in X-ray Photoelectron Spectroscopy of Polymers,” *Anal. Chem.*, vol. 64, no. 15, pp. 1729–1736, 1992, doi: 10.1021/ac00039a018.

[57] C. Satriano, G. M. L. Messina, S. Carnazza, S. Guglielmino, and G. Marletta, “Bacterial adhesion onto nanopatterned polymer surfaces,” *Mater. Sci. Eng. C*, vol. 26, no. 5–7, pp. 942–946, 2006, doi: 10.1016/j.msec.2005.09.096.

[58] S. Carnazza, G. Marletta, M. Frasca, L. Fortuna, and S. Guglielmino, “Spatial patterns of microbial retention on polymer surfaces,” *J. Adhes. Sci. Technol.*, vol. 25, no. 17, pp. 2255–2280, 2011, doi: 10.1163/016942411X574943.

[59] L. S. Shi, L. Y. Wang, and Y. N. Wang, “The investigation of argon plasma surface modification to polyethylene: Quantitative ATR-FTIR spectroscopic analysis,” *Eur. Polym. J.*, vol. 42, no. 7, pp. 1625–1633, 2006, doi: 10.1016/j.eurpolymj.2006.01.007.

[60] N. De Geyter, R. Morent, and C. Leys, “Surface characterization of plasma-modified polyethylene by contact angle experiments and ATR-FTIR spectroscopy,” *Surf. Interface Anal.*, vol. 40, no. 3–4, pp. 608–611, 2008, doi: 10.1002/sia.2611.

[61] R. Morent, N. De Geyter, S. Van Vlierberghe, P. Dubruel, C. Leys, and E. Schacht,

"Organic-inorganic behaviour of HMDSO films plasma-polymerized at atmospheric pressure," *Surf. Coatings Technol.*, vol. 203, no. 10–11, pp. 1366–1372, 2009, doi: 10.1016/j.surfcoat.2008.11.008.

[62] A. S. Meshkova, Y. Liu, F. M. Elam, S. A. Starostin, M. C. M. van de Sanden, and H. W. de Vries, "The role of the gradient film properties in silica moisture barriers synthesized in a roll-to-roll atmospheric pressure plasma enhanced CVD reactor," *Plasma Process. Polym.*, vol. 15, no. 1, pp. 1–10, 2018, doi: 10.1002/ppap.201700093.

[63] M. Goldstein, *Infrared characteristic group frequencies*, vol. 5, no. 2. 1981.

[64] F. Fanelli, F. Fracassi, and R. d'Agostino, "Atmospheric pressure PECVD of fluorocarbon coatings from glow dielectric barrier discharges," *Plasma Process. Polym.*, vol. 4, no. SUPPL.1, pp. 430–434, 2007, doi: 10.1002/ppap.200731201.

[65] N. M. Mackie, N. F. Dalleska, D. G. Castner, and E. R. Fisher, "Comparison of Pulsed and Continuous-Wave Deposition of Thin Films from Saturated Fluorocarbon/H2 Inductively Coupled rf Plasmas," *Chem. Mater.*, vol. 9, no. 1, pp. 349–362, 1997, doi: 10.1021/cm960388q.

[66] J. Fang, L. Zhang, D. Sutton, X. Wang, and T. Lin, "This is the published version : Available from Deakin Research Online : Needleless Melt-Electrospinning of Polypropylene Nanofibres," 2012, doi: 10.1155/2012/382639.

[67] T. J. Lenk *et al.*, "Structural Investigation of Molecular Organization in Self-Assembled Monolayers of a Semifluorinated Amidethiol," *Langmuir*, vol. 10, no. 12, pp. 4610–4617, 1994, doi: 10.1021/la00024a037.

[68] R. M. Romano, J. Czarnowski, and C. O. Della Védova, "Preparation and conformational properties of the perfluoro diether CF3OCF2OCF2C(O)F, a model molecule to study properties of perfluoro polyethers," *Inorg. Chem.*, vol. 40, no. 13, pp. 3039–3047, 2001, doi: 10.1021/ic0008520.

[69] L. Martinů, H. Biederman, and J. Nedbal, "Dielectric properties of fluorocarbon and chlorofluorocarbon films plasma polymerized in an R.F. glow discharge," *Thin Solid Films*, vol. 136, no. 1, pp. 11–19, 1986, doi: 10.1016/0040-6090(86)90103-3.

[70] V. Y. Osipov, N. M. Romanov, K. Kogane, H. Touhara, Y. Hattori, and K. Takai, "Intrinsic infrared absorption for carbon–fluorine bonding in fluorinated nanodiamond," *Mendeleev Commun.*, vol. 30, no. 1, pp. 84–87, 2020, doi: 10.1016/j.mencom.2020.01.028.

[71] D. P. Dowling, C. E. Nwankire, M. Riihimäki, R. Keiski, and U. Nylén, "Evaluation of the anti-fouling properties of nm thick atmospheric plasma deposited coatings," *Surf.*

Coatings Technol., vol. 205, no. 5, pp. 1544–1551, 2010, doi: 10.1016/j.surfcoat.2010.10.010.

[72] H. Giegengack and D. Hinze, "Investigations of the structure of thin fluorocarbon films by x-ray diffraction and infrared spectroscopy," *Phys. Status Solidi*, vol. 8, no. 2, pp. 513–520, 1971, doi: 10.1002/pssa.2210080221.

[73] J. J. Senkevich and D. W. Sherrer, "Plasma enhanced chemical vapor deposition of fluorocarbon thin films via CF3H/H2 chemistries: Power, pressure, and feed stock composition studies," *J. Vac. Sci. Technol. A Vacuum, Surfaces, Film.*, vol. 18, no. 2, pp. 377–384, 2000, doi: 10.1116/1.582196.

[74] K. K. S. Lau, J. A. Caulfield, and K. K. Gleason, "Structure and morphology of fluorocarbon films grown by hot filament chemical vapor desposition," *Chem. Mater.*, vol. 12, no. 10, pp. 3032–3037, 2000, doi: 10.1021/cm000499w.

[75] K. P. Huang, P. Lin, and H. C. Shih, "Structures and properties of fluorinated amorphous carbon films," *J. Appl. Phys.*, vol. 96, no. 1, pp. 354–360, 2004, doi: 10.1063/1.1755849.

[76] B. Karmakar, *Fundamentals of Glass and Glass Nanocomposites*. Elsevier Inc., 2016.

[77] L. Adumeau, C. Genevois, L. Roudier, C. Schatz, F. Couillaud, and S. Mornet, "Impact of surface grafting density of PEG macromolecules on dually fluorescent silica nanoparticles used for the in vivo imaging of subcutaneous tumors," *Biochim. Biophys. Acta - Gen. Subj.*, vol. 1861, no. 6, pp. 1587–1596, 2017, doi: 10.1016/j.bbagen.2017.01.036.

[78] M. Inayoshi, M. Hori, T. Goto, M. Hiramatsu, M. Nawata, and S. Hattori, " Formation of polytetrafluoroethylene thin films by using CO 2 laser evaporation and XeCl laser ablation ," *J. Vac. Sci. Technol. A Vacuum, Surfaces, Film.*, vol. 14, no. 4, pp. 1981–1985, 1996, doi: 10.1116/1.580071.

[79] A. Fidalgo and L. M. Ilharco, "The defect structure of sol-gel-derived silica/polytetrahydrofuran hybrid films by FTIR," *J. Non. Cryst. Solids*, vol. 283, no. 1–3, pp. 144–154, 2001, doi: 10.1016/S0022-3093(01)00418-5.

[80] H. Sanaeishoar, M. Sabbaghan, and F. Mohave, "Synthesis and characterization of micro-mesoporous MCM-41 using various ionic liquids as co-templates," *Microporous Mesoporous Mater.*, vol. 217, pp. 219–224, 2015, doi: 10.1016/j.micromeso.2015.06.027.

[81] M. N. Chai and M. I. N. Isa, "The Oleic Acid Composition Effect on the Carboxymethyl Cellulose Based Biopolymer Electrolyte," *J. Cryst. Process Technol.*, vol. 03, no. 01, pp. 1–4, 2013, doi: 10.4236/jcpt.2013.31001.

[82] X. Zhu, F. Arefi-khonsari, C. Petit-etienne, and M. Tatoulian, “Open Air Deposition of SiO 2 Films by an Atmospheric Pressure Line-Shaped Plasma,” pp. 407–413, 2005, doi: 10.1002/ppap.200400049.

[83] B. Shokri, M. A. Firouzjah, and S. I. Hosseini, “FTIR analysis of silicon dioxide thin film deposited by metal organic-based PECVD,” *Proc. 19th Int. Plasma Chem. Soc.*, pp. 1–4, 2009, doi: www.ispc-conference.org.

[84] “Annex 1 - FTIR spectroscopy,” .

[85] Y. Sawada, S. Ogawa, and M. Kogoma, “Synthesis of plasma-polymerized tetraethoxysilane and hexamethyldisiloxane films prepared by atmospheric pressure glow discharge,” *J. Phys. D. Appl. Phys.*, vol. 28, no. 8, pp. 1661–1669, 1995, doi: 10.1088/0022-3727/28/8/015.

[86] M. T. Kim, “Deposition behavior of hexamethydisiloxane films based on the FTIR analysis of Si-O-Si and Si-CH3 bonds,” *Thin Solid Films*, vol. 311, no. 1–2, pp. 157–163, 1997, doi: 10.1016/S0040-6090(97)00683-4.

[87] F. Babonneau, K. Thorne, and J. D. Mackenzie, “Dimethyldiethoxysilane / Tetraethoxysilane Copolymers : Precursors for the Si-C-O System,” no. 10, pp. 554–558, 1989.

[88] Y. Kawano and S. C. De Araujo, “Raman and infrared spectra of polychlorotrifluoroethylene,” *Journal of the Brazilian Chemical Society*, vol. 7, no. 6. pp. 491–496, 1996, doi: 10.5935/0103-5053.19960088.

[89] E. Herth, R. Zeggari, J. Y. Rauch, F. Remy-Martin, and W. Boireau, “Investigation of amorphous SiOx layer on gold surface for Surface Plasmon Resonance measurements,” *Microelectron. Eng.*, vol. 163, no. October 2017, pp. 43–48, 2016, doi: 10.1016/j.mee.2016.04.014.

[90] J. F. Moulder, W. F. Stickle, P. E. Sobol, and K. D. Bomben, “Handbook of X-ray Photoelectron Spectroscopy Edited by,” *Google Sch.*, pp. 1–261, 1993, [Online]. Available: https://books.google.com/books/about/Handbook_of_X_ray_Photoelectron_Spectros.html?hl=fr&id=A_XGQgAACAAJ.

[91] X. L. Zhu *et al.*, “Analysis by using X-ray photoelectron spectroscopy for polymethyl methacrylate and polytetrafluoroethylene etched by KrF excimer laser,” *Appl. Surf. Sci.*, vol. 253, no. 6, pp. 3122–3126, 2007, doi: 10.1016/j.apsusc.2006.07.002.

[92] G. Nansé, E. Papirer, P. Fioux, F. Moguet, and A. Tressaud, “Fluorination of carbon blacks: An X-ray photoelectron spectroscopy study: I. A literature review of XPS studies

of fluorinated carbons. XPS investigation of some reference compounds," *Carbon N. Y.*, vol. 35, no. 2, pp. 175–194, 1997, doi: 10.1016/S0008-6223(96)00095-4.

[93] C. Tudisco *et al.*, "Covalent functionalization of silicon surfaces with a cavitand-modified salen," *Eur. J. Inorg. Chem.*, no. 13, pp. 2124–2131, 2011, doi: 10.1002/ejic.201001239.

[94] C. R. Crick and I. P. Parkin, "Preparation and characterisation of super-hydrophobic surfaces," *Chem. - A Eur. J.*, vol. 16, no. 12, pp. 3568–3588, 2010, doi: 10.1002/chem.200903335.

[95] M. A. Gilliam, Q. Yu, and H. Yasuda, "Plasma polymerization behavior of fluorocarbon monomers in low-pressure AF and RF discharges," *Plasma Process. Polym.*, vol. 4, no. 2, pp. 165–172, 2007, doi: 10.1002/ppap.200600076.

SUPPORTING INFORMATION

Additional supporting information is available in the online version of this article at the publisher's website or from the author.

Video S1:

Figure S1:

FIGURES AND TABLES

FIGURE 1. [Figure Caption.]

Reproduced with permission.[Ref.] Copyright Year, Publisher.

TABLE 1. [Table Caption.]

Head 1 [units][a)]	Head 2	Head 3	Head 4	Head 5 [units]
Column 1	Column 2	Column 3[b)]	Column 4	Column 5
Column 1	Column 2	Column 3	Column 4	Column 5

[a)]((Table Footnote)); [b)] …

Graphical Abstract

Supporting Information

Title

Author(s), Corresponding Author(s)*